DEVELOPMENT OF A HIGHER-ORDER UPWIND ALGORITHM FOR DISCONTINUOUS COMPRESSIBLE FLOW

THESIS

Barry A. Croker, 1LT, USAF

AFIT/GAE/ENY/05-M05

DEPARTMENT OF THE AIR FORCE
AIR UNIVERSITY

AIR FORCE INSTITUTE OF TECHNOLOGY

Wright-Patterson Air Force Base, Ohio

AFIT/GAE/ENY/05-M05

DEVELOPMENT OF A HIGHER-ORDER UPWIND ALGORITHM FOR DISCONTINUOUS COMPRESSIBLE FLOW

THESIS

Presented to the Faculty

Department of Aeronautics and Astronautics

Graduate School of Engineering and Management

Air Force Institute of Technology

Air University

Air Education and Training Command

In Partial Fulfillment of the Requirements for the

Degree of Master of Science in Aeronautical Engineering

Barry A. Croker, B.S.M.E

1LT, USAF

March 2005

AFIT/GAE/ENY/05-M05

DEVELOPMENT OF A HIGHER-ORDER UPWIND ALGORITHM FOR DISCONTINUOUS COMPRESSIBLE FLOW

Barry A. Croker, B.S.M.E

1LT, USAF

Approved:

/signed/	21 Mar 2005
Maj Richard J. McMullan, Ph.D. (Chairman)	date
/signed/	21 Mar 2005
Lt Col Raymond C. Maple, Ph.D. (Member)	date
/signed/	21 Mar 2005
Lt Col Eric J. Stephen, Ph.D. (Member)	date

AFIT/GAE/ENY/05-M05

Abstract

The use of compact differences to discretize partial differential equations produces higher orders of accuracy with a smaller stencil and lower absolute error than approximations using traditional finite differences. However, most solution algorithms for the compressible Euler equations that include compact differencing cannot be applied to problems involving discontinuities (such as shock or contact surfaces) without the use of filtering or limiting methods. A global fourth-order method that incorporates compact differencing with Roe's approximate Riemann solver was investigated. This method was incorporated into a one-dimensional numerical simulation of the compressible Euler equations, and applied to a one-dimensional shock tube problem. The method was also extended to two dimensions, and applied to a two-dimensional shock tube problem and an advecting vortical structure problem on both rectilinear and curvilinear meshes. The results were compared to a third-order Roe scheme and a fourth-order compact difference scheme. The compact Roe scheme was found to be consistent in both the one-dimensional and two-dimensional simulations. An order of accuracy determination showed that it has an order of accuracy somewhere near fourth order, with absolute error comparable to that of the standard compact difference scheme. With proper selection of solution parameters, the scheme was also shown to accurately capture a discontinuous solution where unfiltered compact schemes would become unstable.

Acknowledgements

I would like to give many thanks to my advisor Maj. Richard McMullan for the countless hours he spent listening to my questions as I wrote this thesis, and for the assistance that he offered while troubleshooting my code. I also would like to thank my sponsor Dr. Datta Gaitonde of AFRL/VAAC for his continual guidance and encouragement in my research, especially when I wasn't sure things were going to work the way I thought they should. I owe a debt of gratitude to my dear wife and family, for enduring the long hours without me and for helping me put my thoughts into words that others could understand. Last, but but certainly not least, I offer my sincere gratitude to my Father in Heaven for the strength and opportunity He has given me to participate in this program with so many other devoted individuals. The content of this thesis might one day be forgotten, but the friendships that it has brought about will last a lifetime.

Barry A. Croker

Table of Contents

Page

Abstract iv

Acknowledgements v

List of Figures viii

List of Tables x

List of Symbols xi

List of Abbreviations xv

I. Introduction 1-1
- 1.1 Modeling The Governing Equations of Fluid Flow 1-1
- 1.2 Discretization of the Governing Equations 1-2
- 1.3 Finite Difference and Compact Difference Approximations . . . 1-2
- 1.4 Advantages of the Compact Difference 1-5
- 1.5 Problems with Compact Differencing 1-6
- 1.6 Development of an Upwind Compact-Difference Formulation . 1-7

II. Governing Equations 2-1
- 2.1 1D Linear Wave Equation 2-1
- 2.2 1D Euler Equations 2-1
- 2.3 2D Euler Equations 2-4

III. Numerical Methods 3-1
- 3.1 Formulation of the Compact Difference 3-1
- 3.2 Boundary Conditions 3-3
- 3.3 Application to the 1D Linear Wave Equation 3-4
- 3.4 Application to the 1D Euler Equations 3-5
- 3.5 Roe's Approximate Riemann Solver 3-6
- 3.6 Roe's Scheme in Two Dimensions 3-8
- 3.7 Higher-Order Approximations 3-11
- 3.8 Variable Limiters 3-12
- 3.9 Upwind Compact Formulations 3-13
- 3.10 Implicit Variable Interpolation 3-15
- 3.11 Time Integration 3-17

Page

IV. Results of Solutions to Model Problems 4-1
4.1 Linear Wave Equation 4-1
4.1.1 Setup Conditions 4-1
4.1.2 Linear Wave Equation Results 4-2
4.2 1D Shock Tube 4-4
4.2.1 Problem Description 4-4
4.2.2 Exact Riemann Solution to the Sod Problem 4-5
4.2.3 Setup Conditions 4-7
4.2.4 1D Shock Tube Results 4-8
4.2.5 Accuracy of the cRoe Solution Applied to the 1D Shock Tube 4-10
4.2.6 Variation of the cRoe κ Parameter in the 1D shock tube 4-11
4.2.7 Consistency of the 1D cRoe Scheme 4-13
4.3 2D Shock Tube 4-14
4.3.1 Problem Description and Setup Conditions 4-14
4.3.2 2D Shock Tube Results 4-14
4.3.3 Consistency of the 2D cRoe scheme 4-14
4.3.4 Variation of the cRoe κ Parameter in the 2D Shock Tube 4-14
4.4 Advection of a Vorticial Structure on a Rectilinear Mesh . . . 4-17
4.4.1 Problem Description 4-17
4.4.2 Exact Solution to the Vortex Problem 4-18
4.4.3 Setup Conditions 4-18
4.4.4 Periodic Boundary Condition 4-18
4.4.5 Results to the Vortex Problem 4-20
4.4.6 Order of Accuracy Determination 4-29
4.5 Advection of a Vortical Structure on a Curvilinear Mesh 4-32
4.5.1 Problem Description and Setup Conditions 4-32
4.5.2 Curvilinear Vortex Advection Results 4-33
4.5.3 Order of Accuracy Determination on Curvilinear Mesh 4-41
4.5.4 Variation of cRoe κ Parameter in Vortex Problem . . 4-42

V. Conclusions 5-1
5.1 Strengths of the cRoe scheme 5-2
5.2 Weaknesses of the cRoe scheme 5-2
5.3 Relative Computational Costs 5-3
5.4 Future Work 5-3
5.5 Final Conclusion 5-4

Bibliography 5

Vita VITA-1

List of Figures

Figure		Page
2.1	Discontinuous Solutions to the Rankine-Hugoniot Relations	2-6
4.1	Solutions to the Linear Wave Equation after 64 timesteps, $\nu = 0.5$ . .	4-2
4.2	Error in Solutions to the Linear Wave Equation after 64 timesteps, $\nu = 0.5$	4-3
4.3	Shock Tube Flow State at t = 0	4-4
4.4	Shock Tube Flow State at $t > 0$	4-6
4.5	Comparison of Density Distribution in 1D Shock Tube Problem at $t = 0.16$.	4-8
4.6	Comparison of Velocity Distribution in 1D Shock Tube Problem at $t = 0.16$.	4-9
4.7	Detail of Shock Capture of Roe Method, Density	4-10
4.8	Detail of Normal Shock in Comparison of Solutions to 1D Shock Tube Problem at $t = 0.16$.	4-11
4.9	Variation in κ Parameter for 1D Shock Tube Problem, Detail of Contact Surface Discontinuity	4-12
4.10	cRoe Solution Consistancy to 1D Shock Tube Problem	4-13
4.11	Comparison of Density Distribution in 2D Shock Tube Problem at $t = 0.16$.	4-15
4.12	cRoe Solution Consistancy to 2D Shock Tube Problem	4-16
4.13	Variation in κ Parameter for 2D Shock Tube Problem, Detail of Contact Surface Discontinuity	4-16
4.14	Mesh Overlap on Periodic Boundaries	4-19
4.15	Vorticity Profiles of Advecting Vortex at T=30.0, $\Delta x/R$=0.20	4-21
4.16	Comparison of oRoe Solutions to Vortex Problem along centerline after $t = 30$.	4-23
4.17	Comparison of cC Solutions to Vortex Problem along centerline after $t = 30$.	4-24

Figure Page

4.18 Comparison of cRoe Solutions to Vortex Problem along centerline after $t = 30$. 4-25

4.19 Comparison of Error in oRoe Solutions to Vortex Problem along centerline after $t = 30$. 4-26

4.20 Comparison of Error in cC Solutions to Vortex Problem along centerline after $t = 30$. 4-27

4.21 Comparison of Error in cRoe Solutions to Vortex Problem along centerline after $t = 30$. 4-28

4.22 Order of Accuracy of Solution Methods 4-29

4.23 $\Delta x/R = 0.2$ Curvilinear Mesh with 5-point Overlap 4-33

4.24 Comparison of oRoe Solutions to Vortex Problem on a Curvilinear Mesh Along Centerline After $t = 30$. 4-35

4.25 Comparison of cC Solutions to Vortex Problem on a Curvilinear Mesh Along Centerline After $t = 30$. 4-36

4.26 Comparison of cRoe Solutions to Vortex Problem on a Curvilinear Mesh Along Centerline After $t = 30$. 4-37

4.27 Comparison of Error in oRoe Solutions to Vortex Problem on a Curvilinear Mesh Along Centerline After $t = 30$. 4-38

4.28 Comparison of Error in cC Solutions to Vortex Problem on a Curvilinear Mesh Along Centerline After $t = 30$. 4-39

4.29 Comparison of Error in cRoe Solutions to Vortex Problem on a Curvilinear Mesh Along Centerline After $t = 30$. 4-40

4.30 Order of Accuracy of Solution Methods on a Curvilinear Mesh 4-41

4.31 Variation in κ parameter for cRoe problem, $\Delta x/R = 0.4$ 4-43

List of Tables

Table		Page
3.1	Various Values of Parameters from Equation (3.1)	3-2
3.2	Various Values of Parameters from Equation (3.46)	3-16
3.3	Various Values of Parameters from Equation (3.47)	3-16
4.1	Theoretical and Calculated Orders of Accuracy for Various Solution Methods	4-29
4.2	Theoretical and Calculated Orders of Accuracy for Various Solution Methods on a Curvilinear Mesh	4-41

List of Symbols

Symbol Page

Constants

γ ratio of specific heats 11

R universal gas constant 11

Greek Symbols

α Runge-Kutta coefficient 31

α compact difference coefficient 7

β compact difference coefficient 15

Δ difference operator 2

δ difference operator 21

∇ divergence operator 22

∂ partial differential operator 2

ϵ Roe entropy correction coefficient 22

η generalized coordinate 13

κ interpolant switch weighting factor 29

κ variable extrapolation constant 26

λ eigenvalue 21

ν Courant number 9

n wave frequency 63

ϕ phase shift angle 63

ρ density 10

ξ generalized coordinate 13

Roman Symbols

A Jacobian of transformation 20

A wave amplitude 63

a compact difference coefficient 7

a speed of sound 19

a wave propagation speed 9

b compact difference coefficient 15

C shock propagation speed 36

c compact difference coefficient 15

D difference operator 29

d compact difference coefficient 17

e lele resolving efficiency 5

E_t total energy 10

$\mathcal{F}$ flux vector in ξ-direction 13

$\hat{F}$ Roe averaged flux vector in x- or ξ-direction 7

F flux vector in x-direction 10

F initial function 9

f dependent variable 2

$\mathcal{G}$ flux vector in η-direction 13

H enthalpy 20

$\hat{i}$ principle axis unit vector 14

ii number of grid points in x-direction 63

$\hat{j}$ principle axis unit vector 14

J inverse of cell interface area 13

jj number of grid points in y-direction 63

K interpolant switch parameter 29

k wavenumber constant 5

L reference length 35

n Number of points in domain 4

n number of timesteps 9

O order of accuracy 18

P shock tube pressure ratio 36

p pressure 10

R Roe density ratio 20

R residual vector 31

R vortex core radius 48

r vortex radius 48

$\vec{S}$ outward facing unit normal 11

T temperature 11

t time 9

TV total variation 26

$\mathcal{U}$ contravariant velocity in ξ-direction 22

U conservative variable vector 10

u component of velocity in x-direction 10

$\mathcal{V}$ contravariant velocity in η-direction 22

$\forall$ control cell volume 11

V primitive variable vector 25

v component of velocity in y-direction 12

v primitive variable 25

x coordinate of principle axis 9

x independent variable 2

y coordinate of principle axis 12

z Roe quadratic parameter 20

Superscripts

i index notation 3

$_L$ left cell interface 26

o evaluation point 2

$\pm\frac{1}{2}$ interface 7

$_R$ right cell interface 26

θ coordinate direction of principle axis 48

x differentiation with respect to x 13

y differentiation with respect to y 13

Subscripts

$^-$ Roe averaged value 21

$'$ First derivative of dependent variable 4

∞ freestream value 48

$^\sim$ Roe averaged value 20

^{T} vector transpose 25

List of Abbreviations

Abbreviation		Page
PDE	Partial Differential Equation	1-1
TSE	Taylor Series Expansion	1-2
LES	Large Eddy Simulation	1-4
DNS	Direct Numerical Simulation	1-4
LWE	Linear Wave Equation	2-1
MUSCL	Montone Upwind-centered Scheme for Conservation Laws	3-11
TVD	Total Variation Diminishing	3-12
ENO	Essentially Non-Oscillatory	3-15
CFL	Courant-Friedrichs-Lewy Number	4-18

DEVELOPMENT OF A HIGHER-ORDER UPWIND ALGORITHM FOR DISCONTINUOUS COMPRESSIBLE FLOW

I. Introduction

1.1 Modeling The Governing Equations of Fluid Flow

The governing equations of fluid flow are hyperbolic, non-linear, partial differential equations (PDE) of multiple variables. They are continuum statements of conservation of mass, momentum and energy, which can describe the flow of any Newtonian fluid under almost any circumstance. They were originally proposed by Leonhard Euler in the mid 1750's, and later refined by Claude Louis Marie Henri Navier in the early 1820's. Nearly two hundred years later, their work still remains somewhat unfinished. Because of the complexity of these governing equations, no generalized closed-form, exact solutions have been discovered [1].

For years scientists and engineers relied on various methods to approximate the solutions to these equations. Many of these solutions were limited to specialized or idealized cases, with simplifications necessary to bring the problem closure. The advent of the computer age opened a new chapter in the field of solving these differential equations. No longer did solutions have to be simplified and terms ignored to be solved. Computers allowed the governing equations to be approximated through various linearization and discritization techniques and to be solved numerically.

As one can imagine, these numerical solution techniques do not involve trivial computations. Current computer technology has yet to advance to the point that many complex flow problems can be fully modeled and accurately solved. However, the technology to solve what was once a daunting problem for a fluid engineer can now be approximated quite accurately by anyone who possesses a personal computer.

In their most general form, the governing equations have two major components—partial derivatives with respect to time (temporal derivatives), and partial derivatives with

respect to space (spatial derivatives). The temporal derivatives are somewhat straightforward to approximate, as time only increases in one dimension and in an orderly fashion. The real challenge is in developing an accurate approximation to the spatial derivative terms. The methods chosen to approximate the spatial derivatives are highly dependent on the problem being solved. They are influenced by the problem geometry, the flow conditions, and even the fluids involved.

1.2 Discretization of the Governing Equations

These governing equations are continuum statements, which means they can describe physical phenomena at any point in space at any time. The first step in trying to approximate them is to discretize them, or divide them up into finite portions in space and time. The value of a continuous function at a discrete point in space can be approximated by the value of the function and its derivatives at other discrete points. This approximation is called a Taylor Series Expansion (TSE). For example, the TSE of a function f at $(x_o + \Delta x)$ can be expressed as a function of the value at x_o and the derivatives of f at x_o.

$$f(x_o + \Delta x) = f(x_o) + \left.\frac{\partial f}{\partial x}\right|_{x_o} \Delta x + \left.\frac{\partial^2 f}{\partial x^2}\right|_{x_o} \frac{\Delta x^2}{2!} + \left.\frac{\partial^3 f}{\partial x^3}\right|_{x_o} \frac{\Delta x^3}{3!} + \ldots + \left.\frac{\partial^n f}{\partial x^n}\right|_{x_o} \frac{\Delta x^n}{n!} \quad (1.1)$$

Because of the factorial terms in the denominator, a TSE is a converging series. If the TSE included an infinite number of terms it would produce the exact value of f. Since only a finite number of terms can actually be used, the approximation has an error term associated with it. The magnitude of the exponent on Δx in the last term of the TSE is called the order of the expansion.

1.3 Finite Difference and Compact Difference Approximations

If the terms in the TSE are re-arranged, discrete approximations for the derivative terms can be developed. The exact value of the derivative can be expressed as the sum of a finite-difference expression and a truncation error. For example, if the first derivative term is moved to the left-hand side and solved for, the result is an expression of the first

derivative $\partial f/\partial x$ as a function of the values of f at two known points:

$$\frac{\partial f}{\partial x} = \frac{f(x_o + \Delta x) - f(x_o)}{\Delta x} + \frac{\partial^2 f}{\partial x^2}\frac{\Delta x}{2!} + \dots \tag{1.2}$$

The finite-difference expression is the first term on the left-hand side, while the truncation error is an infinite series beginning with the $\partial^2 f/\partial x^2$ term. This finite-difference approximation is first-order, as Δx in the leading truncation error term has an exponent of one. If terms in the truncation error are replaced with other finite-difference expressions, higher accuracy approximations can be derived. For example, a fourth order accurate representation of the first derivative of the variable f at point i could be expressed as:

$$\frac{\partial f_i}{\partial x} = \frac{f_{i-2} - 8f_{i-1} + 8f_{i+1} - f_{i+2}}{12\Delta x} + O(\Delta x)^4 \tag{1.3}$$

In essence, the derivative at a point is determined by a curve fit through the values at surrounding points. In this case, the finite difference expression is a central difference where information from either side is used to determine the slope at the point in question. Finite differences can also be one sided, either forwards or backwards, using information from only one direction.

Since the governing PDEs consist of multiple partial derivatives, these discretized derivatives can be substituted and numerical approximations made. Additional work is needed for the linearization of certain terms, but the underlying methodology remains the same: continuous functions are replaced with discretized representations, each having their associated truncation error. The combined influence of the individual truncation errors results in an overall order of accuracy of the solution.

Higher order solutions result in better approximations due to both the magnitude of the truncation error and the rate at which the truncation error approaches zero. Since the truncation error is a function of Δx, the accuracy of the solution is often dependent on the refinement of the mesh. Since most solution meshes have values of $\Delta x < 1$, the higher the order the approximation the smaller the truncation error terms. When comparing two solutions of different orders a higher order approximation allows for better resolution

and accuracy of flow structures and behaviors without the need of a greatly refined grid. Conversely, a low order approximation on a coarse grid will be more prone to error than a higher order one would be on the same grid.

In recent years, advances in computing power have allowed methods such as large eddy simulation (LES) and direct numerical simulation (DNS) to gain popularity. Both of these methods attempt to numerically solve the governing equations of turbulent fluid flow completely from large to very small scales. Since many turbulent problems involve complex flow patterns and very small length scales, these methods require considerable computing power and highly refined meshes. First or second order approximations often cannot resolve the high frequencies and miniscule length scales involved in these types of simulations. Information propagating at the high frequencies is overcome by the truncation error terms, and the solution begins to break down. Small scale flow structures are dissipated out and the turbulent structures are lost.

Traditional finite differences can in theory be derived for any accuracy, but in practice they are limited to second or third order. The order of a finite difference is related to the number of points included in the "stencil", or function points used in the calculation. This number of points also increases with the degree of the derivative. For example, for a given accuracy a second derivative needs more points than a first derivative. A wider stencil not only requires a more complicated solution algorithm but can cause complications at boundaries of the solution domain.

An alternate approach to gaining higher order approximations without as large a stencil size is through the use of Padé, or compact, finite difference methods [15]. In the compact formulation, the value of the derivative f' is still expressed as a function of the surrounding values of f, but in an implicit relation. For example, a fourth-order representation of the first derivative f' can be expressed as

$$\frac{1}{4}f'_{i-1} + f'_i + \frac{1}{4}f'_{i+1} = \frac{3}{4}\frac{f_{i+1} - f_{i-1}}{\Delta x} + O(\Delta x)^4 \tag{1.4}$$

In this case the unknowns are the f' terms on the left-hand side of the equation, while the known values are on the right-hand side. For a domain $1 < i < n$, a system of n equations can be written and solved simultaneously for n unknown values of f'. In this case the

number of points in the approximation has been reduced from five points to three, making the stencil more "compact".

1.4 Advantages of the Compact Difference

One major advantage of using compact difference methods, aside from having a smaller stencil, is an increase in solution resolution over traditional finite difference methods. Information in a hyperbolic domain propagates via waves of characteristics. A Fourier decomposition of a solution would show a broad spectrum of waves from large to small wavenumbers. Certain portions of the flow structure rely on different portions of this spectrum to propagate information. Large scale eddys transport energy through the low frequency waves, while turbulent scales dissipate energy at the high frequencies. As previously stated, it is these high-frequency waves that are the most challenging to model. Lele [15] defines a resolving efficiency as the ratio of the maximum wave number for a well resolved wave ($|k\Delta x| \leq \pi$) to the theoretically existing Fourier wavenumbers. Whereas traditional fourth-order differences have a resolving efficiency near $e = 0.19$, a compact formulation efficiency is closer to $e = 0.477$ [12]. This means nearly twice as much high-frequency information is captured by the compact-difference as by the finite-difference. Additionally, compact difference methods also exhibit smaller phase speed errors further resulting in better resolution of high wavenumber flow features. Both of these features mean that an LES or DNS solution using compact-differencing will almost always produce a more accurate solution than one using traditional finite-differences.

Another consequence of using compact difference methods is a decrease in the magnitude of the truncation error, and hence an additional increase in the overall accuracy of the solution. While a finite-difference and a compact-difference scheme could both have a truncation error term of the same order, the magnitude of this term is generally smaller for the compact case. Because of this difference in absolute error, a fourth order compact scheme of the first derivative can have a Δx of $6^{\frac{1}{4}} \approx 1.57$ larger than a standard fourth order finite difference expression while maintaining the same accuracy [16].

1.5 Problems with Compact Differencing

With better high wavenumber resolution, lower overall error, and a smaller stencil, the compact difference at first appears to be a superior method for spatial discretization. For the approximation of a linear function this is usually the case, but one must remember the PDE's which govern generalized fluid flow are highly non-linear, and additional considerations must be taken. The right-hand side of a compact difference such as equation 1.4 uses information from before and after the desired evaluation point, i.e. for f'_i the values of f_{i-1} and f_{i+1} are needed. This "before and after" is termed a central difference, in this case centered at i. For non-linear problems which contain discontinuous solutions, central difference methods are unconditionally unstable and will oscillate without bound. This is caused by the fact that the characteristic information only propagates in a single direction. If information is incorporated from a location that is downstream of the direction of the characterics, non-physical behavior will result. Since the compact-difference scheme uses a central difference term on the right-hand side, it is unusable for problems containing discontinuities, specifically problems involving shock waves.

One method which allows compact differences to be used with such problems is to use spectral-like filtering methods to remove non-physical oscillations. These spectral filters remove the unbounded high-frequency oscillations before they have a negative impact on the overall solution. To be efficient, a spectral filter should have twice the order of accuracy as that of the solution method [5]. For example, on a fourth-order solution, an eight or higher order filter would be required. Not only do these high-order filters require a large stencil, they are computationally expensive and add considerably to the complexity of the solution. An alternate method, which is the goal of this thesis, is to incorporate an upwind bias into the compact difference formulation and eliminate the sources of oscillations altogether.

An upwind bias means that the solution method only uses information that is relevant—information that is "upwind" of the point in question. An upwind bias for the previous example could be the value of f'_i would depend on f_{i-1} and f_{i-2}, while not considering f_{i+1}. Even with the use of standard finite differences, upwind biasing is necessary for an accurate, physical solution. If upwinding could be incorporated into a compact difference scheme, a global higher-order solution could be developed that would forgo the use of filters. Work

by Ravichandran [18] demonstrated that it is feasible to incorporate the upwinding into the compact formulation using flux vector splitting, where the sign of the flux Jacobians determines the direction of information propagation. However, the derived scheme in itself is not non-oscillatory, and requires the use of limiters at solution extrema.

1.6 Development of an Upwind Compact-Difference Formulation

It was suggested by David Gottlieb [7] that using an upwind flux-differencing scheme, such as Roe's scheme, directly into a compact formulation such as Equation 1.4 could allow for a stable higher order solution method without the use of filters. Fluxes would be calculated using Roe's scheme, then substituted directly into the compact scheme to produce a higher order approximation of $\partial f/\partial x$. Since many existing numerical simulations include a Roe flux solver, this could imply that higher-order solutions could be calculated readily without a new solution algorithm. This proposition could be summarized as follows:

$$\alpha\hat{F}'_{i-1} + \hat{F}'_i + \alpha\hat{F}'_{i+1} = \frac{a}{\Delta x}(\hat{F}_{i+1/2} - \hat{F}_{i-1/2}) \tag{1.5}$$

where $\hat{F}$ denotes Roe averaged fluxes, and

$$\begin{aligned} a =& \frac{3}{8}(3 - 2\alpha) \\ \alpha =& \frac{1}{22} \end{aligned}$$

Preliminary investigation shows that this solution formulation is only partially correct. While the once unconditionally-unstable compact scheme of Equation 1.4 is now made stable, it appears to only have overall order the same as the order of the flux calculations. Hence, if $\hat{F}$ is calculated to first order the compact formulation will only produce first order $\hat{F}'$ values. Deng and Maekawa [3] have developed a fourth-order compact variable interpolation scheme which appears to allow method Equation 1.5 to be globally fourth order. Their findings only present results in one-dimension and attempt no verification of the formal order of accuracy of the new method.

It is the goal of this thesis to investigate the proposition of Gottlieb and to better understand the new method of Deng and Maekawa [3]. This new "cRoe" method is based

on compact-difference methods and Roe's approximate Riemann solver, but forgoes the use of spectral filters through the use of an adaptive compact variable interpolant. The development of the regular compact difference will first be discussed. This compact method will then be applied to a model linear equation in one-dimension and compared with a first-order explicit method. Next, the cRoe method will be applied to a one-dimensional discontinuous Riemann problem and compared with a third-order Roe scheme (oRoe). The cRoe scheme will then be extended to two-dimensions and applied to a similar Riemann problem. These Riemann problems will allow for a measure of the consistency of the hybrid cRoe scheme while also allowing a comparison with the oRoe method. Next, the cRoe method will be compared with the third-order oRoe and a fourth-order compact differencing scheme (cC) on a problem involving the advection of a vortical structure on a rectilinear mesh. This problem will allow the formal order of accuracy of the cRoe solution to be determined and the absolute error to be compared to the oRoe and cC schemes. Finally, the three methods will be applied to the same vortex problem on a curvilinear mesh to gain a more realistic measure of the usefulness of the solution methods.

II. Governing Equations

In order to understand the behavior of various schemes involving both compact and finite differences several model problems will be considered. To verify the validity of the compact difference formulation a linear one-dimensional problem will first be investigated.

2.1 1D Linear Wave Equation

The 1-D linear wave equation (LWE) [21]:

$$\frac{\partial f}{\partial t} + a\frac{\partial f}{\partial x} = 0 \tag{2.1}$$

(or advection equation) is a hyperbolic partial differential equation that describes the motion of a wave moving in the x direction at a velocity a. It also can describe the convective transport of a scalar quantity f at a flow speed a [11]. It's exact solution is described by

$$f(x,t) = F(x - a\Delta t) \tag{2.2}$$

given initial data

$$f(x,0) = F(x) \quad -\infty < x < \infty \tag{2.3}$$

The LWE is a useful tool which can model the transportive behavior of the equations that govern generalized fluid flow. Since the LWE is linear and scalar it is much simpler to use than fully non-linear vectorized equations. Solution methods for nonlinear equations are often initially applied to the LWE as a preliminary form of validation. If a solution is unstable when applied to the LWE it will almost certainly be unstable on a more complex problem. However, if a solution is stable when applied to the LWE it could be worth investigating with a more complex equation set such as Eulers equations.

2.2 1D Euler Equations

The Euler Equations are the governing equations for compressible inviscid fluid flow. They consist of two scalar equations for conservation of mass and energy and one vector equation for conservation of momentum. All three equations form a first order system of coupled non-linear partial differential equations (PDEs).

The Euler equations can be written in a number of equivalent forms based on the derivation method used. If a PDE can be expressed having constant coefficients on the derivative terms, (or if the coefficients are variable the derivatives appear only once), the formulation is said to be in "conservation form". "Divergence form" is also an acceptable description for a physical conservation law with divergence terms of physical quantities. [21]. In order to compute a correct solution for a discontinuous flow the conservation form of the governing equations must be used [11].

Two sets of variables are be used in the conservation form of the Euler equations: conservative variables and primitive variables. Conservative variables are the conserved quantities that the equations are derived from: conservation of mass, momentum and energy. Primitive variables are those that can be experimentally measured and are often imposed by the physical domain of the problem, i.e. density ρ, velocity u, and pressure p. Written in one-dimensional, conservative, differential form the Euler set is given as [11]:

$$\frac{\partial U}{\partial t} + \frac{\partial F}{\partial x} = 0 \tag{2.4}$$

The vector of conserved variables U and vector of conserved fluxes F can be expressed in terms of the primitive variables as

$$U = \begin{bmatrix} \rho \\ \rho u \\ E_t \end{bmatrix}, F = \begin{bmatrix} \rho u \\ \rho u^2 + p \\ (E_t + p)u \end{bmatrix} \tag{2.5}$$

Equation 2.4 is a system of three equations with four unknowns: ρ, u, p, and E_t. To reach closure an additional equation of state is added which relates the thermodynamic properties of the fluid. One common assumption is that of a calorically perfect gas such that

$$p = \rho \mathcal{R} \mathcal{T} \tag{2.6}$$

where $\mathcal{R}$ is the universal gas constant and T is the temperature. With this assumption total energy can be calculated using

$$E_t = \frac{p}{\gamma - 1} + \frac{1}{2}\rho u^2 \tag{2.7}$$

where γ is the ratio of specific heats. For this thesis the fluid considered will be air with γ=1.4 and $\mathcal{R}$=287 N m/kg K.

The Equation 2.4 can be used directly to solve the Euler set using a finite difference solution method. A finite-difference solution method computes the solution to a flow by looking at the changes in the conserved variables at discrete points in space and time. The system of PDE's described by Euler's equations represent continuum solutions which at any point in time or space represent a statement of conservation. In order to reach a solution to these equations finite-difference expressions can be made that well approximate the PDE at a localized point. If these approximations individually represent the actual solution it is expected that the global solution will also closely match the exact solution and the method is said to have a conservative property [21]. As more and more points are added to the solution method these approximations become closer and closer to the exact value of the PDE and solution method is said to be consistent [21].

An alternate solution method can be derived from looking not only at the PDE as a mathematical expression but as a description of a physical phenomena. If an arbitrary control volume is taken in the solution domain it can be shown that the time rate of change of the conserved variables within the control volume is equal to the net flux through the control volume boundary [11]. In this method the Euler equations in integral form are

$$\frac{\partial}{\partial t}\int_{\forall} U d\forall + \int_s F\hat{i} \cdot d\vec{S} = 0 \tag{2.8}$$

where U and F have the same definitions as the previous form. This result could also be reached by taking the differential form of Equation 2.4 and applying the divergence theorm [11].

A finite-volume solution method uses this integral form to divide the computational domain into a mesh of discrete cells. As the size of the control volumes are reduced, i.e the

mesh is refined, it is expected that the approximate value in the control volume approaches it's exact value and the method is again considered to be consistent.

In order for Equation 2.8 to be conservative, it must hold true for any sized control volume. This means that a finite-volume solution method does not require a uniform computational domain. Since most physical flow problems cannot be easily discretized with a uniform mesh a finite volume method is useful for "real world" problems [11].

2.3 2D Euler Equations

When extended to two dimensions the Euler set changes slightly due to an additional degree of freedom. Whereas in one dimension there was only a single velocity, in two dimensions there are two separate velocity components: u in the x direction and v in the y direction. Combined with mass these two velocities make up two separate momentums which must be individually conserved. Additionally, whenever a velocity is considered in an energy term the total vector sum of u and v must now be taken into account.

When developing a solution method in more than a single direction it is often useful to define a localized coordinate system for each discrete point in the domain [21]. The conservative variables and fluxes can be calculated as a function of the unit vectors of the local coordinates. For an arbitrary curvilinear domain the local normal coordinate system at each point or control volume will not necessarily align itself with the cartesian coordinates system. However, a coordinate transformation can be developed such that the physical domain is mapped to the local computational (cartesian) domain. This transformation is done through the use of "grid metrics", defined as

$$\begin{aligned} \frac{\xi_x}{J} &= \frac{\partial y}{\partial \eta} \\ \frac{\xi_y}{J} &= -\frac{\partial x}{\partial \eta} \\ \frac{\eta_x}{J} &= -\frac{\partial y}{\partial \xi} \\ \frac{\eta_y}{J} &= \frac{\partial x}{\partial \xi} \\ J &= \xi_x \eta_y - \xi_y \eta_x \end{aligned} \tag{2.9}$$

where the $[x, y]$ domain is the physical domain and the $[\xi, \eta]$ is the computational domain. The term J in two dimensions can be considered as the inverse of the cell area. It is often convenient to specify that the computational domain is uniform such that $\Delta\xi = \Delta\eta = 1$. In this manner a non-uniform curvilinear physical domain can be transformed into a uniform rectilinear computational domain. Using these definitions for grid metrics the Euler equations can be written in generalized coordinate differential form as

$$\frac{1}{J}\frac{\partial U}{\partial t} + \frac{\partial \mathcal{F}}{\partial \xi} + \frac{\partial \mathcal{G}}{\partial \eta} = 0 \tag{2.10}$$

where $\mathcal{F}$ and $\mathcal{G}$ are the conservative flux vectors such that

$$\begin{aligned} \mathcal{F} &= \frac{\xi_x}{J}F + \frac{\xi_y}{J}G \\ \mathcal{G} &= \frac{\eta_x}{J}F + \frac{\eta_y}{J}G \end{aligned} \tag{2.11}$$

The conservative variable vector U and flux vectors F and G can also be expressed in terms of the primitive variables

$$U = \begin{bmatrix} \rho \\ \rho u \\ \rho v \\ E_t \end{bmatrix}, F = \begin{bmatrix} \rho u \\ \rho u^2 + p \\ \rho uv \\ (E_t + p)u \end{bmatrix}, G = \begin{bmatrix} \rho u \\ \rho uv \\ \rho v^2 + p \\ (E_t + p)v \end{bmatrix} \tag{2.12}$$

Finally, the equation of state is again used for closure such that with an ideal gas total energy may be calculated as

$$E_t = \frac{p}{\gamma - 1} + \frac{1}{2}\rho(u^2 + v^2) \tag{2.13}$$

As with one-dimension, it is often beneficial to express the Euler set in conservative integral form for use in a finite-volume method. Using the same definition of ρ, u, v and p it can be shown that the corresponding integral form is

$$\frac{\partial}{\partial t}\int_{\forall} U d\forall + \int_s (F\hat{i} + G\hat{j}) \cdot d\vec{S} = 0 \tag{2.14}$$

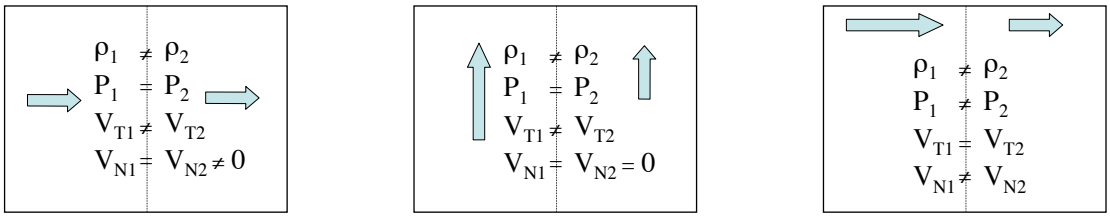

(a) Contact Surface (b) Slip Line (c) Shock Surface

Figure 2.1: Discontinuous Solutions to the Rankine-Hugoniot Relations

Eulers equations allow for both strong (continuous) and weak (discontinuous) solutions [11]. Strictly speaking, the differential form of Eulers equations requires a solution with smoothness or one with continuous derivatives. In order to capture the weak solutions an integral form must be used. It can be shown that the Euler set allows three types of discontinuous solutions, all of which satisfy the Rankine-Hugoniot jump conditions: contact surfaces, slip lines, and shock surfaces (Figure 2.1). Contact surfaces are defined where there is a discontinuity in density, but pressure and velocity are continuous. At the interface between the two states a boundary exists with zero mass flow across it. Slip lines are similar to contact surfaces, but there also exists a discontinuity in tangential velocity across the boundary while pressure and normal velocity remain continuous. The third solution, with mass flow across the boundary, is a shock surface where pressure, density, and normal velocity all experience discontinuities. For the shock surface tangential velocity remains continuous across the shock.

Since stagnation pressure is not constant across a shock, entropy likewise is discontinuous. Mathematically the Euler equations allow for the existence of a condition where the change in entropy across a discontinuity could be negative, forming an "expansion shock" of sorts. However, this result would be in violation of the second law of thermodynamics: that the change in entropy of a system must always be greater than or equal to zero. A valid solution technique must therefore be able to enforce this constraint due to the second law thus avoiding non-physical behavior.

In the next chapter the numerical schemes to solve the linear wave equation and the Euler equations will be presented.

III. Numerical Methods

The Linear Wave Equation and Euler's Equations (both one and two dimensional) are hyperbolic PDE's of two or more independent variables. In order to reach a numerical solution they must be separated into two distinct portions: spatial terms (x, y) and temporal terms (t). A common solution method consists of first calculating a linearized spatial term at a given time then integrating explicitly with respect to time to reach a solution at the next time step. This process is then repeated until the desired end state is reached. In order to calculate the spatial terms the equations must first be discretized or simplified for evaluation at a finite number of discrete points in a computational domain.

3.1 Formulation of the Compact Difference

The compact difference begins with a generalized 7-point implicit stencil [12]:

$$\beta f'_{i-2} + \alpha f'_{i-1} + f'_i + \alpha f'_{i+1} + \beta f'_{i+2} = a\frac{f_{i+1} - f_{i-1}}{2\Delta x} + b\frac{f_{i+2} - f_{i-2}}{4\Delta x} + c\frac{f_{i+3} - f_{i-3}}{6\Delta x} \quad (3.1)$$

where

$$f'_i = \frac{\partial f_i}{\partial x} \quad (3.2)$$

If TSE's for f_i, f_{i+1}, etc. are substituted into Equation 3.1 a system of equations can then be written such that the coefficients a,b and c cause desired terms of the TSE to cancel. Solving this system of equations will produce the coefficients needed for an implicit expression for f' with a truncation error consisting of the remaining terms. Using this method the fourth order representation of the first derivative becomes:

$$\frac{1}{4}f'_{i-1} + f'_i + \frac{1}{4}f'_{i+1} = \frac{3}{4}\frac{f_{i+1} - f_{i-1}}{\Delta x} + O(\Delta x)^4 \quad (3.3)$$

This particular compact stencil will be henceforth referred to as the "cC" compact scheme. Note that the stencil has been reduced from 5 points for a traditional finite difference (i-2 through i+2, see Equation 1.3) to 3 points (i-1 through i+1). Other values for these coefficients and their respective orders are summarized in Table 3.1.

These formulations are all based on the assumption that the value of the function f and the desired derivative f' reside at the same discretized locations. This methodology can

also be used when f and f' are not co-located assuming the appropriate TSE's are used. For example, in a finite-volume discretization scheme the values of a flux f might be known at cell interfaces while the change in flux $\partial f/\partial x$ would be desired at the cell centers. TSE's for the right hand side would be expanded about $i \pm 1/2$ whereas TSE's for the left-hand side would be expanded about $i-1$, i, and $i+1$. Again, a system of equations can be written in terms of α, β, a, b, and c such that desired terms in each TSE cancel. The remaining TSE terms make up the truncation error. Using this method a fourth order set of coefficients using these interface values could be calculated using:

$$\alpha f'_{i-1} + f'_i + \beta f'_{i+1} = \frac{a}{\Delta x} f_{i+\frac{1}{2}} - \frac{b}{\Delta x} f_{i-\frac{1}{2}} \tag{3.4}$$

with

$$\begin{aligned} a =& \frac{3}{4}(\alpha + \beta) \\ b =& \frac{1}{6}(\alpha + \beta) \end{aligned}$$

All of these stencils produce an implicit formulation for the value of f'. The resulting solution matrix is sparse, but banded. The left-hand side coefficients α and β are free parameters which determine the solution matrix type. For $\beta = 0$ and $2\alpha < 1$ the resulting matrix is diagonally dominant and tri-diagonal which can be easily solved using the Thomas algorithm [10]. For eighth and higher order schemes $\beta \neq 0$ and the resulting matrix is penta-diagonal which must be solved using other methods.

For this thesis, the fourth-order version of Equation 3.1 was used for the cC scheme and the implicit operator was a diagonally-dominant tri-diagonal system. A low-storage version of the Thomas algorithm [21] was then employed. The Thomas algorithm is essentially

Table 3.1: Various Values of Parameters from Equation (3.1)

α	β	a	b	c	Order
α	0	$\frac{2}{3}(\alpha+2)$	$\frac{1}{3}(4\alpha-1)$	0	4^{th}
α	0	$\frac{1}{6}(\alpha+9)$	$\frac{1}{15}(32\alpha-9)$	$\frac{1}{10}(1-3\alpha)$	6^{th}
α	$\frac{1}{20}(8\alpha-3)$	$\frac{1}{6}(12-7\alpha)$	$\frac{1}{150}(568\alpha-183)$	$\frac{1}{50}(9\alpha-4)$	8^{th}

Gaussian elimination modified to take advantage of the sparse matrix. The implicit operator is first put into upper triangular form by computing new diagonal elements. The second step computes new right-hand values based on this upper triangular matrix. The final step is to back-substitute and compute the unknown values. Since the only non-zero terms of the left-hand matrix are the lower diagonal, diagonal, and upper diagonals, they are the only terms passed to the Thomas subroutine in the form of three column vectors. The Thomas algorithm has the advantage of solving tri-diagonal system very quickly with a minimal number of calculations and storage.

3.2 Boundary Conditions

Compact methods such as Equations 3.1 and 3.3 use a central-difference-like stencil which can lead to difficulties near boundaries. For example, Equation 3.3 is only usable in the domain from $2 < i < n - 1$ where n is the number of known values of f. At the points $i = 1$ and $i = n$ another method must be used since the stencil would reach outside of the solution domain.

For Dirschlet and Neumann boundary conditions ghost cells can be readily extrapolated from the domain and used as known points. For these cases the values of f or f' would be readily known and the value could be moved to the right hand side of the equation.

An alternate method is to use one-sided differences which are derived in a similar manner as Equation 3.1. In this case, the left hand stencil does not extend out of the known domain ($1 \leq i \leq ni$). A one-sided approximation to f' at a minimum boundary ($i = 1$) could be used as:

$$f'_i + \alpha f'_{i+1} = af_i + bf_{i+1} + cf_{i+2} + df_{i+3} \tag{3.5}$$

With $[\alpha, a, b, c, d]$ = [-17/6, 3/2, 3/2, -1/6] the solution is fourth-order. It is worth noting that when the solution becomes one-sided the stencil width of the right hand side increased from three points to four. A tradeoff to widening the right hand side would be to reduce the order of accuracy of the approximation at the boundary.

3.3 Application to the 1D Linear Wave Equation

As previously stated the Linear Wave Equation is given by:

$$\frac{\partial f}{\partial t} + a\frac{\partial f}{\partial x} = 0 \tag{3.6}$$

One possible explicit solution to the linear wave equation is the first-upwind formulation [12]:

$$f_i^{n+1} = f_i^n - \frac{a\Delta t}{\Delta x}(f_i^n - f_{i-1}^n) \tag{3.7}$$

Known values of f at time n are used to explicitly calculate new values of f at $n+1$. In effect both temporal and spatial time steps are calculated at the same time. This method is first order accurate in time and space ($O(\Delta x, \Delta t)$). While this method is simple to implement it introduces a great deal of artificial dissipation for values of $\nu < 1$ (where $\nu = a\Delta t/\Delta x$) which results in a diminishing wave. A more accurate solution would result from using a compact difference method (Equation. 3.3) for the spatial term $\partial f/\partial x$ and then a separate time integration method for the temporal term. To make the spatial integration fourth-order the following formulation was used:

$$\alpha f'_{i-1} + f'_i + \alpha f'_{i+1} = a\frac{f_{i+1} - f_{i-1}}{2\Delta x} + b\frac{f_{i+2} - f_{i-2}}{4\Delta x} \tag{3.8}$$

where

$$\begin{aligned} a =& \frac{2}{3}(\alpha + 2) \\ b =& \frac{1}{4}(3\alpha - 1) \\ \alpha =& \frac{1}{10} \end{aligned} \tag{3.9}$$

Note that Equation 3.9 is used instead of Equation 3.1 so that the left-hand side forms a tridiagonal system of equations. Known values of f at time n are used to make the right hand side of Equation 3.9, then the implicit problem was solved for f' using the Thomas algorithm [21]. The new value of f at time $n+1$ was then determined using a corresponding

fourth-order Runge-Kutta time integration method:

$$\begin{aligned} f_1 &= f^n \\ f_2 &= f^n - \frac{a\Delta t}{4}\frac{\partial f_1}{\partial x} \\ f_3 &= f^n - \frac{a\Delta t}{3}\frac{\partial f_2}{\partial x} \\ f_4 &= f^n - \frac{a\Delta t}{2}\frac{\partial f_3}{\partial x} \\ f^{n+1} &= f^n - a\Delta t\frac{\partial f_4}{\partial x} \end{aligned} \tag{3.10}$$

making the solution globally fourth-order ($O(\Delta x^4, \Delta t^4)$). Note that the implicit system formed by Equation 3.9 needs to be solved at each stage of the Runge-Kutta scheme.

3.4 Application to the 1D Euler Equations

The flux term of the one-dimensional Euler set (Equation 2.4) is a nonlinear transportive term similar to the $\partial f/\partial x$ term of the LWE. The temporal term can be calculated using the Runge-Kutta time integration scheme as was used on the LWE, but the flux term cannot be solved using the same compact difference method due to the inherent design of the compact difference stencil. A major disadvantage of the formulations such as Equation 3.1 or equation 3.3 is that they include central-like difference terms on the right-hand side of the formulation. Central differences when used on nonlinear hyperbolic problems produce unconditionally unstable oscillations around discontinuities. This was not an issue with the LWE which was a scalar linear problem with a single characteristic of a constant sign. The Euler set in one dimension has three characteristics: u, $u + a$, and $u - a$, (where a is the speed of sound). The characteristics are the eigenvalues of the flux Jacobian and dictate the direction and speed of information propagation. For a subsonic problem two of the characteristics will propagate in the flow direction while one will propagate in the opposite direction of the flow. For a supersonic problem all three characteristics run in the flow direction. To maintain stability the solution must take the direction of these characteristics into account and only use values of the function in the upwind or opposite direction of the characteristic.

3.5 Roe's Approximate Riemann Solver

To develop an upwind solution method the one-dimensional Euler equations can be rewritten in non-conservative quasi-linear form in terms of the Jacobian A:

$$\frac{\partial U}{\partial t} + A\frac{\partial U}{\partial x} = 0 \tag{3.11}$$

where the flux Jacobian is

$$A = \frac{\partial F}{\partial U} \tag{3.12}$$

Philip Roe [11] postulated that if A were evaluated at some average interface value ($\tilde{A}$) rather than at cell centers a conservative upwind scheme could be developed such that:

$$\hat{F}_{i+\frac{1}{2}} = \frac{1}{2}(F_i + F_{i+1} - |\tilde{A}|(U_{i+1} - U_i)) \tag{3.13}$$

Roe noted that both the conservative variable vector U and the Euler flux vector F were quadratic functions of a parameter vector z such that

$$z = \sqrt{\rho}\begin{bmatrix} 1 \\ u \\ H \end{bmatrix} \tag{3.14}$$

where ρ is density, u is x-velocity, and H is total enthalpy. Roe then showed using the properties of quadratic functions that the Roe matrix $\tilde{A}$ is exactly the flux Jacobian A, evaluated with Roe-averaged variables. For a one-dimensional system Roe's scheme begins with "Roe-averaged" primitive variables being calculated at cell interfaces using the square root of the product of the densities R

$$\begin{aligned} R_{i+1/2} &= \sqrt{\frac{\rho_{i+1}}{\rho_i}} \\ \tilde{\rho}_{i+1/2} &= R_{i+1/2}\rho_i \\ \tilde{u}_{i+1/2} &= \frac{R_{i+1/2}u_{i+1} + u_i}{R_{i+1/2} + 1} \\ \tilde{H}_{i+1/2} &= \frac{R_{i+1/2}H_{i+1} + H_i}{R_{i+1/2} + 1} \end{aligned} \tag{3.15}$$

The average speed of sound at the interface is then calculated from these values with

$$\tilde{a}^2 = (\gamma - 1)\left(\tilde{H} - \frac{\tilde{u}^2}{2}\right) \tag{3.16}$$

The associated eigenvalues and right eigenvectors to the Roe matrix $\tilde{A}$ are

$$\tilde{\lambda}_{(1)} = \tilde{u} \quad \tilde{\lambda}_{(2)} = \tilde{u} + \tilde{a} \quad \tilde{\lambda}_{(3)} = \tilde{u} - \tilde{a} \tag{3.17}$$

and

$$\tilde{r}^{(1)} = \begin{bmatrix} 1 \\ \tilde{u} \\ \frac{\tilde{u}^2}{2} \end{bmatrix}, \quad \tilde{r}^{(2)} = \begin{bmatrix} 1 \\ \tilde{u} + \tilde{a} \\ \tilde{H} + \tilde{u}\tilde{a} \end{bmatrix} \frac{\tilde{\rho}}{2\tilde{a}}, \quad \tilde{r}^{(3)} = \begin{bmatrix} 1 \\ \tilde{u} - \tilde{a} \\ \tilde{H} - \tilde{u}\tilde{a} \end{bmatrix} \frac{\tilde{\rho}}{2\tilde{a}} \tag{3.18}$$

Next, the wave amplitudes at the interface are calculated using simple averages

$$\begin{aligned} \delta w_1 &= \delta\rho - \frac{\delta p}{\tilde{a}^2} \\ \delta w_2 &= \delta u - \frac{\delta p}{\tilde{\rho}\tilde{a}} \\ \delta w_3 &= \delta u - \frac{\delta p}{\tilde{\rho}\tilde{a}} \\ \delta u_{i+1/2} &= u_{i+1} - u_i \\ \delta p_{i+1/2} &= p_{i+1} - p_i \\ \delta \rho_{i+1/2} &= \rho_{i+1} - \rho_i \end{aligned} \tag{3.19}$$

and finally, the numerical flux $\hat{F}$ is found from

$$\hat{F}_{i+1/2} = \frac{1}{2}\left[(F_i + F_{i+1}) - \sum_j \left|\tilde{\lambda}_j \delta w_j \tilde{r}^j\right|\right] \tag{3.20}$$

where F_i and F_{i+1} are the exact fluxes based on the left and right cell states. When written in the form of Equation 3.20 the summation term can be thought of as an artificial dissipation-like term which was calculated using the appropriate upwind information.

One drawback to Roe's scheme as presented above is that the solution does not see the sonic point and will admit an expansion shock as a valid solution [11]. This non-physical

behavior can be eliminated by the addition of slight artifical dissipation in the calculation of the $\tilde{A}$ eigenvalues. Harten and Hyman [8] suggest the following entropy correction:

$$|\bar{\lambda}|_{mod} = \begin{cases} |\bar{\lambda}|_{i+1/2} & \text{if } |\tilde{\lambda}|_{i+1/2} \geq \epsilon \\ \frac{1}{2}\left(\frac{\tilde{\lambda}^2_{i+1/2}}{\epsilon} + \epsilon\right) & \text{if } |\tilde{\lambda}|_{i+1/2} < \epsilon \end{cases} \tag{3.21}$$

where ϵ is a value such that

$$\epsilon = \max\left[0, (\tilde{\lambda}_{i+1/2}, -\lambda_i), (\lambda_{i+1} - \tilde{\lambda}_{i+1/2})\right] \tag{3.22}$$

3.6 Roe's Scheme in Two Dimensions

When Roe's solution is extended to two dimensions the procedure needs to be modified slightly [23]. Since there is more than one dimension the contravariant velocities $\mathcal{U}$ and $\mathcal{V}$ must be used instead of the vector quantities u and v.

$$\begin{aligned} \mathcal{U} =& \hat{\xi_x} u + \hat{\xi_y} v \\ \mathcal{V} =& \hat{\eta_x} u + \hat{\eta_y} v \\ \hat{\xi_x} =& \frac{\xi_x}{|\nabla \xi|} \\ \hat{\xi_y} =& \frac{\xi_y}{|\nabla \xi|} \\ \hat{\eta_x} =& \frac{\eta_x}{|\nabla \eta|} \\ \hat{\eta_y} =& \frac{\eta_y}{|\nabla \eta|} \end{aligned} \tag{3.23}$$

where $\mathcal{U}$ and $\mathcal{V}$ are the velocity components in the ξ and η directions, respectively. The flux vector in the ξ direction is

$$\hat{\mathcal{F}} = \frac{|\nabla \xi|}{J} \begin{bmatrix} \rho \mathcal{U} \\ \rho \mathcal{U} u + \hat{\xi_x} p \\ \rho \mathcal{U} v + \hat{\xi_y} p \\ (E_t + p)\mathcal{U} \end{bmatrix} \tag{3.24}$$

The Roe vector which is a product of the Roe matrix and the change of conserved variables across the cell interface is given by

$$|\tilde{A}|(U_{i+1}-U_i)) = \frac{|\nabla\xi|}{J}\begin{bmatrix} \alpha_4 \\ \tilde{u}\alpha_4 + \frac{\xi_x}{|\nabla\xi|}\alpha_5 + \alpha_6 \\ \tilde{v}\alpha_4 + \frac{\xi_y}{|\nabla\xi|}\alpha_5 + \alpha_7 \\ \tilde{H}\alpha_4 + \tilde{\mathcal{U}}\alpha_5 + \tilde{u}\alpha_6 + \tilde{v}\alpha_7 - (\frac{\tilde{a}^2}{\gamma-1})\alpha_1 \end{bmatrix} \tag{3.25}$$

where

$$\begin{aligned} \alpha_1 =& |\tilde{\mathcal{U}}|(\Delta\rho - \frac{\Delta p}{\tilde{a}^2}) \\ \alpha_2 =& \frac{1}{2\tilde{a}^2}|\tilde{\mathcal{U}} + \tilde{a}|(\Delta p + \tilde{\rho}\tilde{a}\Delta\mathcal{U}) \\ \alpha_3 =& \frac{1}{2\tilde{a}^2}|\tilde{\mathcal{U}} - \tilde{a}|(\Delta p - \tilde{\rho}\tilde{a}\Delta\mathcal{U}) \\ \alpha_4 =& \alpha_1 + \alpha_2 + \alpha_3 \\ \alpha_5 =& \tilde{a}(\alpha_2 - \alpha_3) \\ \alpha_6 =& |\tilde{\mathcal{U}}|(\tilde{\rho}\Delta u - \frac{\xi_x}{|\nabla\xi|}\tilde{\rho}\Delta\mathcal{U}) \\ \alpha_7 =& |\tilde{\mathcal{U}}|(\tilde{\rho}\Delta v - \frac{\xi_y}{|\nabla\xi|}\tilde{\rho}\Delta\mathcal{U}) \\ \tilde{\mathcal{U}} =& \hat{\xi_x}\tilde{u} + \hat{\xi_y}\tilde{v} \end{aligned} \tag{3.26}$$

Similarly, the flux vector in the η direction is

$$\hat{\mathcal{G}} = \frac{|\nabla\eta|}{J}\begin{bmatrix} \rho\mathcal{V} \\ \rho\mathcal{V}u + \hat{\eta_x}p \\ \rho\mathcal{V}v + \hat{\eta_y}p \\ (E_t+p)\mathcal{V} \end{bmatrix} \tag{3.27}$$

The Roe matrix in this direction is given by

$$|\tilde{A}|(U_{i+1}-U_i)) = \frac{|\nabla\eta|}{J}\begin{bmatrix} \alpha_4 \\ \tilde{u}\alpha_4 + \frac{\eta_x}{|\nabla\eta|}\alpha_5 + \alpha_6 \\ \tilde{v}\alpha_4 + \frac{\eta_y}{|\nabla\eta|}\alpha_5 + \alpha_7 \\ \tilde{H}\alpha_4 + \tilde{\mathcal{V}}\alpha_5 + \tilde{u}\alpha_6 + \tilde{v}\alpha_7 - (\frac{\tilde{a}^2}{\gamma-1})\alpha_1 \end{bmatrix} \tag{3.28}$$

$$
\begin{aligned}
\alpha_1 =& |\tilde{\mathcal{V}}|(\Delta\rho - \frac{\Delta p}{\tilde{a}^2}) \\
\alpha_2 =& \frac{1}{2\tilde{a}^2}|\tilde{\mathcal{V}} + \tilde{a}|(\Delta p + \tilde{\rho}\tilde{a}\Delta\mathcal{V}) \\
\alpha_3 =& \frac{1}{2\tilde{a}^2}|\tilde{\mathcal{V}} - \tilde{a}|(\Delta p - \tilde{\rho}\tilde{a}\Delta\mathcal{V}) \\
\alpha_4 =& \alpha_1 + \alpha_2 + \alpha_3 \\
\alpha_5 =& \tilde{a}(\alpha_2 - \alpha_3) \\
\alpha_6 =& |\tilde{\mathcal{V}}|(\tilde{\rho}\Delta u - \frac{\eta_x}{|\nabla\eta|}\tilde{\rho}\Delta\mathcal{V}) \\
\alpha_7 =& |\tilde{\mathcal{V}}|(\tilde{\rho}\Delta v - \frac{\eta_y}{|\nabla\eta|}\tilde{\rho}\Delta\mathcal{V}) \\
\tilde{\mathcal{V}} =& \eta_x\tilde{u} + \eta_y\tilde{v}
\end{aligned}
\tag{3.29}
$$

The Roe averaged variables are defined in a similar manner as the one-dimension case,

$$
\begin{aligned}
R_{i+1/2} =& \sqrt{\frac{\rho_{i+1}}{\rho_i}} \\
\tilde{\rho}_{i+1/2} =& R_{i+1/2}\rho_i \\
\tilde{u}_{i+1/2} =& \frac{R_{i+1/2}u_{i+1} + u_i}{R_{i+1/2} + 1} \\
\tilde{v}_{i+1/2} =& \frac{R_{i+1/2}v_{i+1} + v_i}{R_{i+1/2} + 1} \\
\tilde{H}_{i+1/2} =& \frac{R_{i+1/2}H_{i+1} + H_i}{R_{i+1/2} + 1}
\end{aligned}
\tag{3.30}
$$

Finally, the Roe fluxes are calculated using

$$
\begin{aligned}
\hat{\mathcal{F}}_{i+\frac{1}{2}} &= \frac{1}{2}(\mathcal{F}_i + \mathcal{F}_{i+1} - |\tilde{A}|(U_{i+1} - U_i)) \\
\hat{\mathcal{G}}_{j+\frac{1}{2}} &= \frac{1}{2}(\mathcal{G}_j + \mathcal{G}_{j+1} - |\tilde{A}|(U_{j+1} - U_j))
\end{aligned}
\tag{3.31}
$$

The same entropy fix as stated in Equation 3.21 was also used to eliminate the possibility of non-physical expansion shocks in the 2D Roe flux calculation.

3.7 Higher-Order Approximations

Roe's method as presented above is a first order approximation in space. In practice this method is too dissipative to be used. Odd-ordered methods tend to have dissipative qualities to them due to the dominance of even-ordered derivative terms in the truncation errors. This, combined with the fact that Roes method uses an artificial dissipation-like term to calculate the upwind fluxes, results in a smearing of gradients and a loss of signal magnitude in solutions.

An improvement comes through the use of Roe's method in conjunction with a variable extrapolation. Roe's method is essentially a weighted average of the flux at a cell interface expressed as a function of the primitive variable vector V ($[\rho, u, p]^T$) in each adjoining cell. A first order approximation assumes that the value of the primitive variable is constant throughout the entire cell with variation only at the cell interfaces. If variation within the cell is allowed a higher order reconstruction can be developed to obtain more accurate left and right primitive variable states at the cell interface.

VanLeer's Montone Upwind-centered Scheme for Conservation Laws [22] (MUSCL) defines a series of piecewise linear approximations to the solution between two cells at the interface. Instituting a TSE about the cell average values for a primitive variable v yields:

$$v_i = \bar{v}_i + (x - x_i)\frac{\partial v}{\partial x}|_i + \frac{(x - x_i)^2}{2}\frac{\partial^2 v}{\partial x^2}\,|_i + O(\Delta x^3) \tag{3.32}$$

where

$$\bar{v}_i = \frac{1}{\Delta x}\int_{x_{i-\frac{1}{2}}}^{x_{i+\frac{1}{2}}} v dx \tag{3.33}$$

Upon simplification, the value for v can be written as

$$v_i = \bar{v}_i + (x - x_i)\frac{\partial \bar{v}}{\partial x} + \frac{1}{2}\frac{\partial^2 \bar{v}}{\partial x^2}\left[(x - x_i)^2 - \frac{\Delta x^2}{12}\right] \tag{3.34}$$

Van Leer chose to scale the last term of this approximation to allow a family of piecewise linear and/or quadratic extrapolation. If central difference approximations are used for the

first and second derivatives the left state cell interface value of v can be calculated using

$$v_L = v_i + \frac{1}{4}(1-\kappa)(v_i - v_{i-1}) + \frac{1}{4}(1+\kappa)(v_{i+1} - v_i) \tag{3.35}$$

and the right state cell interface value of v using

$$v_R = v_{i+1} - \frac{1}{4}(1+\kappa)(v_{i+1} - v_i) - \frac{1}{4}(1-\kappa)(v_{i+2} - v_{i+1}) \tag{3.36}$$

The choice of κ determines the order of the extrapolation. $\kappa = 1/3$ leads to a third-order accurate extrapolation, whereas $\kappa = -1$ would lead to a 3 point fully upwind discretization. To make Equation 3.32 higher order, substitute L and R states for i and $i+1$ respectively. For this thesis, the third-order $\kappa = 1/3$ method will be used and henceforth referred to as "oRoe", or "Original Roe".

3.8 Variable Limiters

Total variation, or the total change in any general solution f is defined as

$$\mathrm{TV} = \int \left| \frac{\partial f}{\partial x} \right| dx \tag{3.37}$$

If this total variation is bounded in both time and space, such that

$$\mathrm{TV}(f^{n+1}) \leq \mathrm{TV}(f^n) \tag{3.38}$$

the solution is said to be total variation diminishing, (TVD) and the following properties of monotonicity hold true [11]: TVD

1. No new local extrema can be created
2. The value of a local minimum is non-decreasing and the value of a local maximum is non-increasing

If these conditions are met the scheme is considered monotone. In essence a TVD scheme is stable such that an introduced perturbation (due to error, etc) in the solution will not grow without bounds, and the solution will remain bounded. While the use of variable extrap-

olation is useful for increasing the order accuracy of a solution it can introduce additional errors due to aliasing and Gibb's effects at gradients and discontinuities [18]. These errors cause solutions to become non-TVD and often cause the solution to diverge. For this reason a limiter is often introduced to enforce the TVD property.

There are various limiter functions which all have a similar purpose: reduce or eliminate non-physical oscillations near solution extrema. In order to work properly the limiter must be used in conjunction with a scheme that is TVD when first order. The limiter functions by extending the scheme to a higher order when the solution is smooth then reverting back to the first-order TVD when the solution is non-smooth. One limiter function which is commonly used is the minmod limiter, defined as [11]

$$\text{minmod}(x,y) = \begin{cases} x & \text{if } |x| < |y| \text{ and } xy > 0 \\ y & \text{if } |x| > |y| \text{ and } xy > 0 \\ 0 & \text{if } xy < 0 \end{cases} \tag{3.39}$$

In compact notation this limiter is often expressed as

$$\text{minmod}(x,y) = \text{sign}(x) \cdot \max[0, \min(|x|, \text{sign}(x \cdot y)] \tag{3.40}$$

In effect the limiter is a switching function to determine how the variable extrapolation is to be constructed. Inherent to their design limiters have the effect of reducing the order of accuracy of the solution near extrema. Because of this behavior variable extrapolation schemes are not of a global order accuracy. This degradation of order is often manifest as a broadening for a shock or a smearing for a contact surface.

3.9 Upwind Compact Formulations

If an upwind bias could be incorporated into a compact-difference method a solution with global higher-order accuracy could theoretically be developed. If the upwinding were done in the proper manner, non-physical behavior could be avoided and the use of limiters or filters would be unnecessary. As previously mentioned it was suggeted by David Gottlieb [7] that a combination of a compact scheme like Equation 3.1 and Roe's scheme could create a higher-order solution with minimal effort.

An investigation of this theory shows that it is only partially correct. Deng and Maekawa [3] show this by beginning with the definition of Roe's scheme,

$$\hat{F}_{i+1/2} = \frac{1}{2}[\hat{F}(U_R) + \hat{F}(U_L) - |\tilde{A}|(U_R - U_L)]_{i+1/2} \tag{3.41}$$

Assuming the left and right states U_L and U_R are interpolated to rth-order accuracy the Roe interface flux becomes

$$\hat{F}_{i+1/2} = \hat{F}(U_{i+1/2}) + d(x_{i+1/2})h^r + O(h^{r+1}) \tag{3.42}$$

and the characteristics of the variable extrapolation scheme and the cell-centered differentiation scheme become one. If Equation 3.42 is substituted back into the compact formulation of Equation 1.5 and TSE's applied at each point i, an expression for $\hat{F}'$ can be shown to be

$$\hat{F}'_i = \left(\frac{\partial \hat{F}}{\partial x}\right)_i + a\frac{d(x_{i+1/2}) - d(x_{i-1/2})}{h}h^r + \frac{17}{5280}\left(\frac{\partial^5 \hat{F}}{\partial x^5}\right)_i h^4 + O(h^6, h^{r+1}) \tag{3.43}$$

Assuming that $d(x)$ is continuous the value of $\hat{F}'$ will be fourth order accurate if $r \geq 4$. If $r < 4$ the value of $\hat{F}'$ will be rth-order accurate. Hence, if the Roe fluxes are only calculated as first order the resulting compact scheme will produce a first order solutions. If variable extrapolation (MUSCL) is used to increase the accuracy of the left and right states to third-order the resulting $\hat{F}$' will also be thrid-order. It is worth noting, however, that Deng and Maekawa [3] did show that the once unconditionally unstable method of Equation 3.1 was now stable without the use of limiters or filters. This is due to the fact that the Roe flux calculations are taking the characteristics into account and are in effect making a compact-upwind method.

The next logical step is to try and increase the order of the variable extrapolations at the left and right interface states to at least fourth-order. This can be accomplished through the use of an implicit interpolation similar in form to a compact difference. However, if the stencil of the interpolant includes a discontinuity the solution will include nonphysical oscillations. If the stencil could be dynamically chosen such that the interpolant stencil avoids discontinuities higher-order reconstruction can be developed without the use of filtering or limiting.

3.10 Implicit Variable Interpolation

Deng and Maekawa [3] developed a method by determining the smoothness of the function that is being interpolated. The absolutes of the first and second Essentially Non-oscillatory (ENO) differences,

$$\begin{aligned} D_{1j} &= v_{j+1} - v_j, \\ D_{2j} &= v_{j+1} - 2v_j + v_{j-1} \end{aligned} \tag{3.44}$$

can be used as a measure of the smoothness of the stencil [9], where v is any primitive variable. The first ENO difference is akin to the slope of the function while the second ENO difference is the curvature of the function. The smaller $|D_1|$ and $|D_2|$ the smoother the function. Using these definitions along with a weighting factor κ, a switch function K for the left and right states can be developed so the compact stencil can be adjusted to avoid discontinuities [3]. For the left state:

$$K_L = \begin{cases} 1, \text{ if } \kappa|D_{1j-1}| \leq |D_{1j}|,\ |D_{2j-1}| < \kappa|D_{2j}|; \\ 3, \text{ if } |D_{1j} < \kappa|D_{1j-1},\ |D_{2j+1}| < \kappa|D_{2j}|; \\ 2, \text{ otherwise.} \end{cases} \tag{3.45}$$

The interpolation for $v_{Lj+1/2}$ is defined as

$$\alpha v_{Lj-1/2} + v_{Lj+1/2} + \beta v_{Lj+3/2} = a v_{j-3} + b v_{j-2} + c v_{j-1} + d v_j + e v_{j+1} + f v_{j+2} + g v_{j+3} \tag{3.46}$$

The resulting values for a, b, c, d, e for a fourth order interpolate of v_L are summarized in Table 3.2.

Similarly for the right state, the interpolation for $v_{Rj+1/2}$ is defined as

$$\alpha v_{Rj-1/2} + v_{Rj+1/2} + \beta v_{Rj+3/2} = a v_{j-3} + b v_{j-2} + c v_{j-1} + d v_j + e v_{j+1} + f v_{j+2} + g v_{j+3} \tag{3.47}$$

Table 3.2: Various Values of Parameters from Equation (3.46)

K_L	α	β	**a**	**b**	**c**	**d**	**e**	**f**	**g**
1	α	β	$\frac{1}{16}(\alpha-5)$	$\frac{1}{16}(21-5\alpha)$	$\frac{1}{16}(15\alpha-35)$	$\frac{1}{16}(5\alpha+35)$	0	0	0
2	$\frac{1}{2}$	$\frac{1}{10}$	0	0	$\frac{1}{10}$	1	$\frac{1}{2}$	0	0
3	α	β	0	0	0	$\frac{1}{16}(5-\beta)$	$\frac{1}{16}(15+9\beta)$	$\frac{1}{16}(9\beta-5)$	$\frac{1}{16}(1-\beta)$

Table 3.3: Various Values of Parameters from Equation (3.47)

K_R	α	β	**a**	**b**	**c**	**d**	**e**	**f**	**g**
1	α	β	0	0	0	$\frac{1}{16}(5\beta+35)$	$\frac{1}{16}(15\beta-35)$	$\frac{1}{16}(21-5\beta)$	$\frac{1}{16}(\beta-5)$
2	$\frac{1}{10}$	$\frac{1}{2}$	0	0	$\frac{1}{2}$	1	$\frac{1}{10}$	0	0
3	α	β	$\frac{1}{16}(1-\alpha)$	$\frac{1}{16}(9\alpha-5)$	$\frac{1}{16}(15+9\alpha)$	$\frac{1}{16}(5-\alpha)$	0	0	0

with the switch function K_R defined as

$$K_R = \begin{cases} 1, \text{ if } \kappa|D_{1j+1}| \leq |D_{1j}|,\ |D_{2j+2}| < \kappa|D_{2j+1}|; \\ 3, \text{ if } |D_{1j} < \kappa|D_{1j+1},\ |D_{2j}| < \kappa|D_{2j+1}|; \\ 2, \text{ otherwise.} \end{cases} \tag{3.48}$$

and the corresponding coefficients determined by K_R shown in Table 3.10.

The parameters α and β are free parameters which determine the form of the left-hand side of the implicit formulation. For this work they were chosen such that $\alpha + \beta < 1$ to maintain a diagonally dominant system that could be also solved with the Thomas algorithm [21]. Deng and Maekawa [3] suggest the weighting factor κ should be chosen $0 \leq \kappa \leq 1$, such that $K_L = 2$ and $K_R = 2$ (a central-type interpolation) is used as much as possible. Since in essence this weighting factor determines when the solution is sufficnetly non-smooth to warrant a one-sided interpolant it is anticipated that the optimal value of κ will vary with each problem the scheme is applied to.

This scheme is called a "Compact Adaptive Interpolation Scheme" by Deng and Maekawa [3]. For the purpose of this thesis, it will be referred to as "cRoe", or the "Compact Roe" scheme.

3.11 Time Integration

Once the numerical Roe flux is known a finite-volume scheme was employed such that the residual R is defined as

$$R_i = \hat{F}_{i+1/2} - \hat{F}_{i-1/2} \tag{3.49}$$

in one dimension, or

$$R_{i,j} = \frac{\hat{\mathcal{F}}_{i+1/2,j} - \hat{\mathcal{F}}_{i-1/2,j}}{\Delta\xi} + \frac{\hat{\mathcal{G}}_{i,j+1/2} - \hat{\mathcal{G}}_{i,j-1/2}}{\Delta\eta} \tag{3.50}$$

in two dimensions. For the compact schemes, solving the implicit matrix results in derivatives of the fluxes directly so that the residual becomes

$$R_i = \frac{\partial\hat{\mathcal{F}}}{\partial\xi} + \frac{\partial\hat{\mathcal{G}}}{\partial\eta} \tag{3.51}$$

Once the residual is determined the time integration of the $\partial U/\partial t$ term can then be accomplished using a four-stage CFD-type Runge-Kutta scheme [13]. This method explicitly solves for the conserved variables at time level $n+1$ given the values at time n using the following four-step process:

$$\begin{aligned} U^0 &= U^n \\ U^k &= U^n - \frac{\alpha_k \Delta t}{\forall} R^{k-1},\ k = 1..3 \\ U^{n+1} &= U^4 \end{aligned} \tag{3.52}$$

where

$$\begin{aligned} \alpha_k &= \frac{1}{5-k} \\ \forall &= \text{cell volume} \end{aligned} \tag{3.53}$$

The "CFD-type" designator refers to the fact that intermediate values of U^k are overwritten each time step instead of being stored at each step as in a traditional Runge-Kutta scheme.

IV. Results of Solutions to Model Problems

In order to better understand the performance of the fourth-order cRoe scheme, several model problems will be investigated. The first step is to verify that the methodology behind the compact-difference formulation is correct, and that there are well-defined advantages to the method. The next step is to duplicate the results of the Compact Adaptive Interpolation (cRoe) Scheme of Deng and Maekawa [3] with respect to the one-dimensional Euler equations. The cRoe scheme will then be extended to two dimensions, and applied to additional problems to understand its behavior and formal order of accuracy. Throughout this process the cRoe results will be compared with the two methods it is derived from: the third-order Roe (oRoe) scheme and the fourth-order compact (cC) scheme.

4.1 Linear Wave Equation

As noted previously, the linear wave equation (LWE) is a one-dimensional scalar equation that can be used to model the transportive behavior of more complex equations. It is often a good starting place for the verification of a new method due to it's simplicity. If the solution method works on the LWE, there is a chance that it will also work on a more complicated set of equations. However, if the method fails on the linear problem it will mostly likely not work on a nonlinear problem.

4.1.1 Setup Conditions. There are various explicit solutions to the LWE, all with different strengths and weaknesses. Tannehill et al. [21] present many of these methods along with an in-depth analysis of the solutions. For simplicity, the solution method considered here was the first-order upwind solution (Equation 3.7). First, a one-dimensional domain of $\Delta x/L = 0.00625$ was used, where Δx is the step size and L is the length of the domain. The domain was initialized with a triangular wave using the following initial conditions:

$$f_o(x) = \begin{cases} 0 & \frac{x}{L} < 0.075 \\ 8.0x - 0.6 & 0.075 \leq \frac{x}{L} \leq 0.2 \\ -8.0x + 2.6 & 0.2 \leq \frac{x}{L} \leq 0.325 \\ 0 & \frac{x}{L} > 0.325 \end{cases} \tag{4.1}$$

The Courant number $\nu = a\Delta t/\Delta x$ was chosen to be 0.5 to ensure solution stability and to demonstrate the dissipative nature of the first-order upwind scheme. The amount of dissipation decreases as ν approaches one. The solution was allowed to progress for $n = 64$ time steps, which ensured the traveling wave remained inside the domain boundaries. The exact solution (Equation 2.2) results in a shift of the initial wave a distance $32\Delta x/L$ to the right, with no decrease in signal amplitude.

This first-order upwind method was compared to a fourth-order compact differencing scheme (Equation 3.9) combined with a fourth-order Runge-Kutta time integration scheme (Equation 3.10) using the same step conditions.

4.1.2 Linear Wave Equation Results. Figure 4.1 compares the results of the first-order and fourth-order methods. Both solutions transported the wave to near the exact location with a small lagging phase error, but it is clear that the compact difference method preserved the shape of the initial triangular wave much better than the first upwind method did. The first upwind method experienced nearly a 30% loss of maximum amplitude while the compact method only lost 5%.

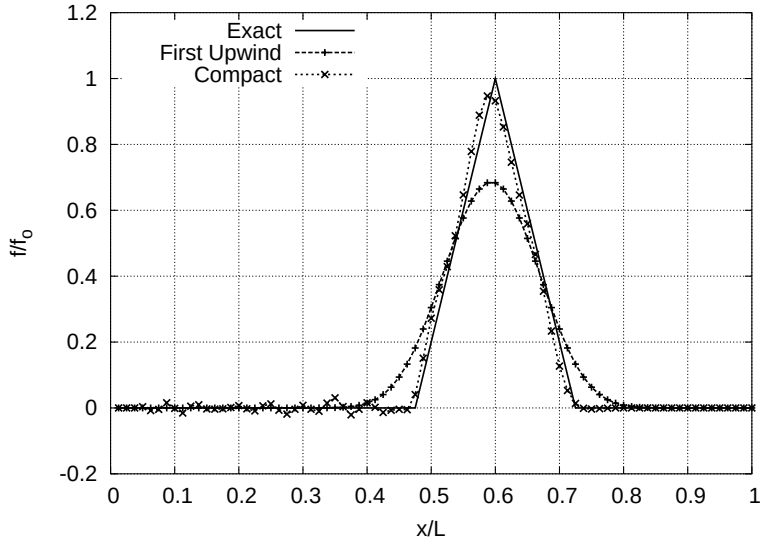

Figure 4.1: Solutions to the Linear Wave Equation after 64 timesteps, $\nu = 0.5$

Figure 4.2 shows the error associated with the two approximations. Again, it is clear that the first order wave introduced a large amount of dissipation error. The greatest amount of error for both solutions was near the peak of the wave where the gradients were the largest, but the compact error was nearly an order of magnitude less than the first upwind method. The higher order compact method did not broaden the base of the wave nor substantially decrease the magnitude of the wave, but it did introduce some dispersion errors (oscillations) before and after the wave. Both of these results can be traced back to the truncation error terms. The first order upwind methods truncation error has a dominant even-ordered derivative which causes dissipation effects while the leading term in the truncation error of the compact method is an odd-ordered derivative and hence dispersive in nature.

Overall, the fourth order compact formulation produced a better approximation of the exact solution. The next step is to extend this compact method to a nonlinear vectorized set of equations and combine it with Roe's approximate Riemann solver.

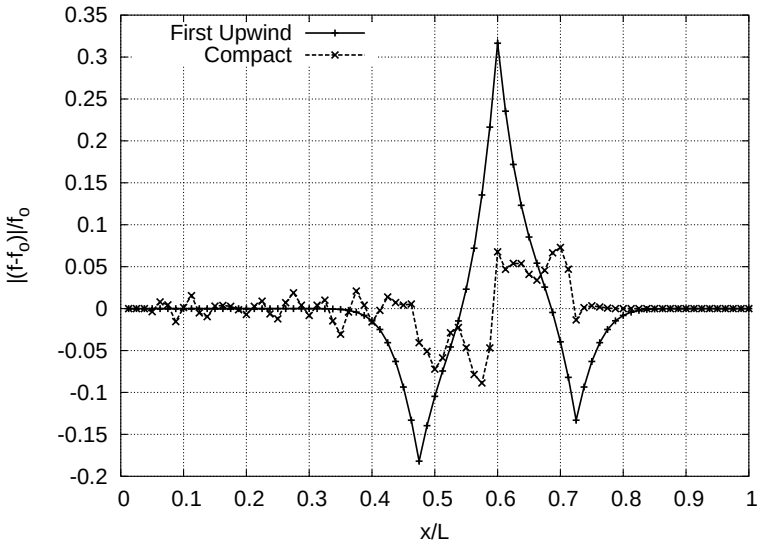

Figure 4.2: Error in Solutions to the Linear Wave Equation after 64 timesteps, $\nu = 0.5$

4.2 1D Shock Tube

4.2.1 Problem Description. The first nonlinear model problem considered was the one-dimensional shock tube problem introduced by Sod [20]. In reality, a shock tube is a three-dimensional problem, but due to planar symmetry can be approximated with a single dimension. The problem consists of a one-dimensional domain of length L. The domain is split into two portions, each of which have different initial conditions (noted as the left and right states) as shown in Figure 4.3. The two portions are isolated until the time $t = 0$ when they are allowed to interact. This problem could be experimentally considered using a gas-filled tube with a thin membrane separating two states. The membrane would be ruptured at $t = 0$ and the two sides would interact.

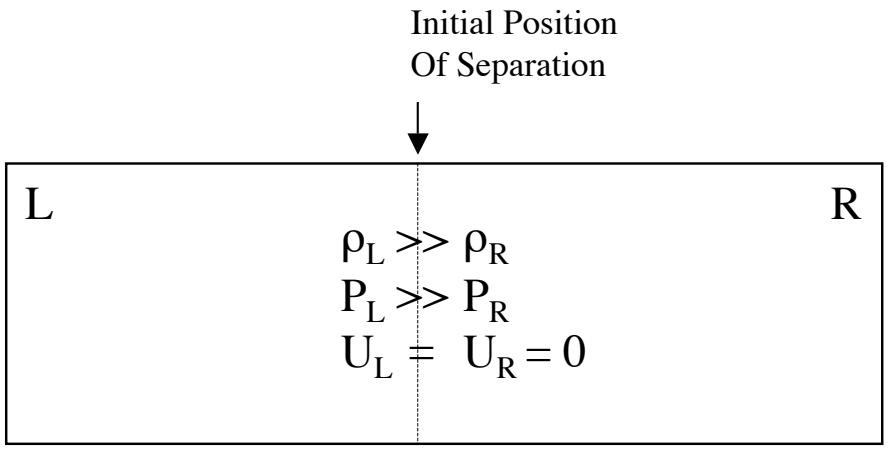

Figure 4.3: Shock Tube Flow State at t = 0

The Riemann solution to this problem allows for the existence of a weak solution, where the value and derivatives of the function can be discontinuous but bounded [11]. For the shock tube problem, there exists two discontinuities: a traveling shock wave due to compression and a contact surface due to the different initial states. The shock is manifest in the solution as a discontinuity in density, velocity, and pressure. The contact surface only appears as a discontinuity in density while pressure and velocity are continuous and constant across it.

At $t = 0$, before the the two states are allowed to interact, the initial velocity is uniformly zero. At $t > 0$ the fluid on the left (high pressure) side of the interface begins to move to the right (low pressure) side of the interface. If the difference in pressure is great enough the compression waves will coalesce into a traveling shock which will travel to the right at the shock propagation speed. At the interface between the two states there will exist a discontinuity in density due to the differences in initial conditions. This discontinuity will also travel to the right at a speed less than the shock propagation speed. As fluid in the the left side of shock tube begins to travel to the right the density in the tube will decrease and an expansion wave will travel from the initial interface to the left side of the tube. This expansion wave is not a discontinuous solution, but could have steep gradients at the leading and trailing edges.

4.2.2 Exact Riemann Solution to the Sod Problem. The flow within the shock tube at a time $t > 0$ is shown in Figure 4.4. The state of the system at $t > 0$ is described by the solution to the Riemann problem [11]. The flow can be divided into five states: the original left (L) and right (R) states, the state between the shock and the contact surface (2), the state between the contact surface and the expansion fan (3), and finally within the expansion fan (5). Using Riemann invariants, an implicit relation for the pressure ratio $P = p_2/p_R$ across the shock can be developed in terms of the left (L) and right (R) states:

$$\sqrt{\frac{2}{\gamma(\gamma-1)}}\frac{P-1}{(1+\alpha P)^{1/2}} = \frac{2}{\gamma-1}\frac{a_L}{a_R}\left[1-\left(P\frac{p_R}{p_L}\right)^{(\gamma-1)/2\gamma}\right]+\frac{u_L-u_R}{a_R} \tag{4.2}$$

with

$$\alpha = \frac{\gamma+1}{\gamma-1} \tag{4.3}$$

Once the pressure ratio across the shock is known the location of the shock at a given point in time can be determined using the propagation speed of the shock (C) in the undisturbed (in this case right) region:

$$C = \frac{(P-1)a_R^2}{\gamma(u_2-u_R)}+u_R \tag{4.4}$$

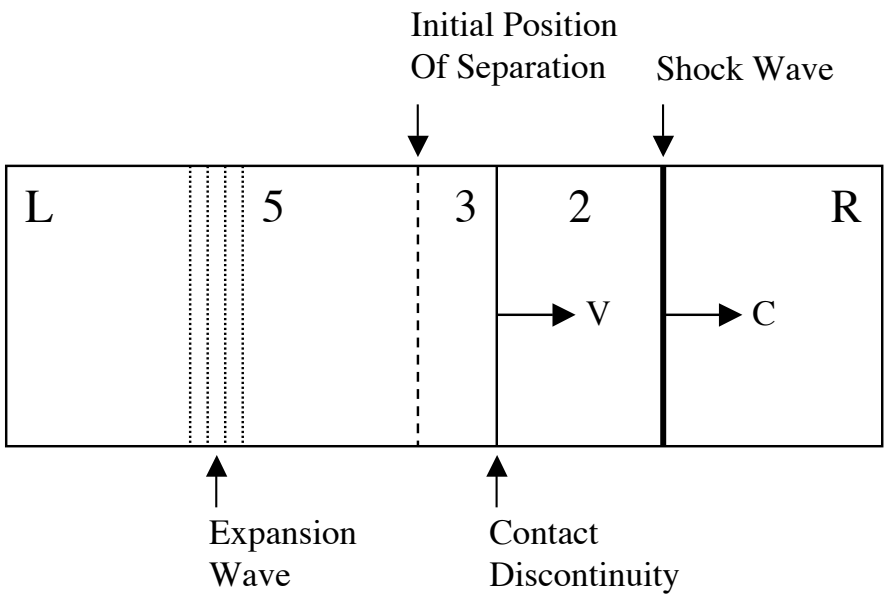

Figure 4.4: Shock Tube Flow State at $t > 0$

The contact surface is a discontinuity in density, but not in pressure or velocity, hence $p_3 = p_2$ and $u_3 = u_2$. This surface travels behind the shock at the constant speed V determined by

$$V = u_2 = \frac{P-1}{\sqrt{(1+\alpha P)}} \frac{a_R}{\sqrt{\gamma(\gamma-1)/2}} + u_R \tag{4.5}$$

The density behind the shock is also a function of the pressure ratio P

$$\rho_2 = \frac{1+\alpha P}{\alpha + P} \rho_R \tag{4.6}$$

The values of the flow variables through the expansion fan (region 5) are determined by the left running characteristics with constant Riemann variables such that

$$\frac{p_5}{\rho_5^\gamma} = \frac{p_L}{\rho_L^\gamma} \tag{4.7}$$

Assuming that the flow is initially at rest ($u_L = u_R = 0$), the velocity throughout the fan varies from zero to V described by

$$u_5 = \frac{2}{\gamma+1}\left(\frac{(x-x_o}{t} + a_L + \frac{\gamma-1}{2}u_L\right)$$
$$\text{for } -\left(\frac{\gamma-1}{2}u_L + a_L\right) < \frac{x-x_o}{t} < \left(\frac{\gamma+1}{2}V - a_L - \frac{\gamma-1}{2}u_L\right) \tag{4.8}$$

Once the velocity distribution is known in region 5 the speed of sound a_5 and pressure p_5 can be expressed in terms of the position in the tube, and time elapsed

$$a_5 = u_5 - \frac{x-x_o}{t}$$
$$p_5 = p_L\left(\frac{a_5}{a_L}\right)^{2\gamma/(\gamma-1)} \tag{4.9}$$

4.2.3 Setup Conditions. For this problem the initial conditions were as follows:

	ρ	u	p
Left	1.0	0.0	1.0
Right	0.125	0.0	0.1

The grid spacings were varied from $\Delta x/L = 5E$-03 to $3.125E$-04. The non-dimensional time step was kept constant at $1.0E$-04. The oRoe method used a MinMod flux limiter, while the cRoe scheme used a κ of 0.3 (this particular choice of κ will be discussed later in this section). The solution was allowed to progress until $t = 0.16$ to keep the shock and expansion waves within the computational domain. Boundary conditions were enforced by flux-fixing the first and last four cells within the domain to zero.

The fourth-order cRoe solves systems of implicit equations twice per Runge-Kutta stage: once for the left and right variable state interpolation, and then again to solve for the spatial derivatives from Equation 1.5. Both of these steps used the Thomas tri-diagonal algorithm [21] to solve the implicit matrices. The results of the cRoe scheme were then compared to both the third-order oRoe scheme and a first-order Roe scheme (fRoe). This comparison was made to show the dissipative effects of a first order solution. The fourth-order cC compact scheme was not considered for this problem since it is unconditionally unstable for a discontinuous (shock) solution.

4.2.4 1D Shock Tube Results. Figures 4.5 and 4.6 show the density and velocity distributions, respectively, within the shock tube at $t = 0.16$. In the density distribution the three distinct features of the flow are readily visible. The density at the far left and far right sides of the domain remain at their initial states, 1.0 and 0.1 respectively. The density then decreases through the expansion wave, and is then constant until approximatly $x/L = 0.65$ at the contact discontinuity. The density again remains constant until the shock near $x/L = 0.78$. In the velocity distribution the left and right states remain at the initial (zero) condition while the fluid in the middle of the domain is moving. The velocity distribution across the expansion wave is again nearly linear while the shock has a steep discontinuity. Unlike the density distribution, the contact surface is not visible in the velocity field since normal velocity is constant across it. All of these flow features are in agreement with the exact solution.

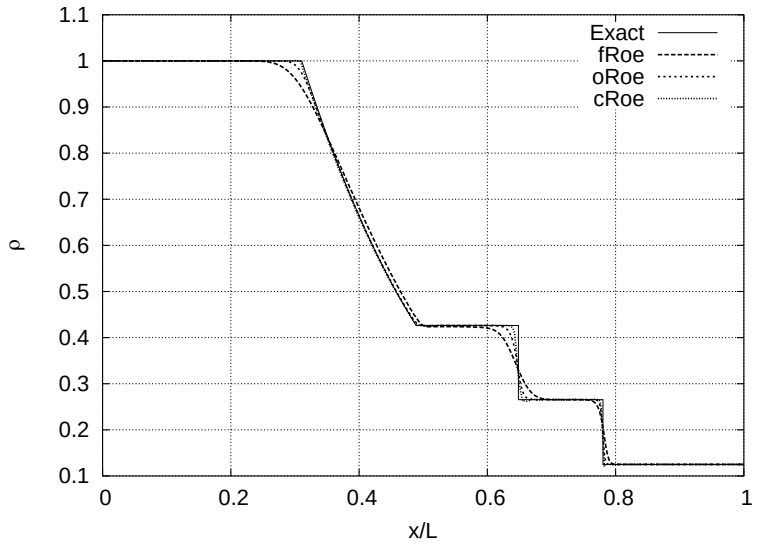

Figure 4.5: Comparison of Density Distribution in 1D Shock Tube Problem at $t = 0.16$.

As expected, the first-order Roe scheme performed the worst with a great deal of dissipation at every location a gradient exists. The corners near the expansion wave are diminished, more so at the left edge than the right. The contact surface is flatted at both ends and the shock is contained (captured) within 17 cells for the $\Delta x/L = 0.025$ case (see

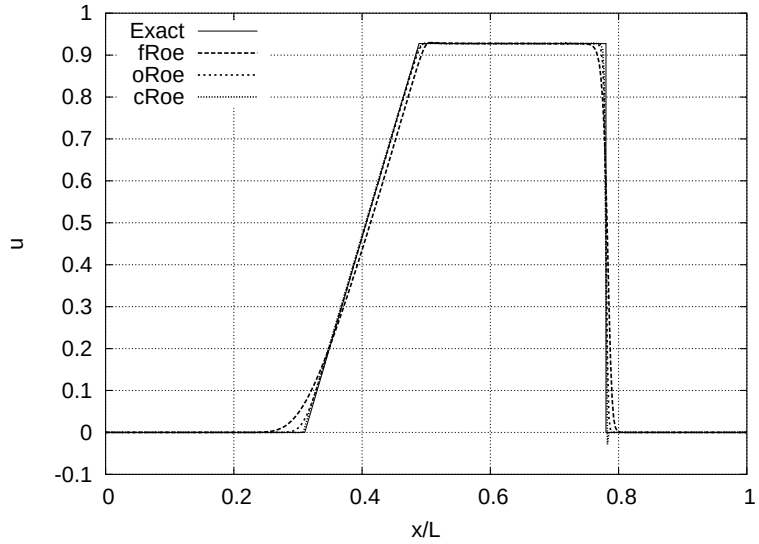

Figure 4.6: Comparison of Velocity Distribution in 1D Shock Tube Problem at $t = 0.16$.

Figure 4.7). Similar to the behavior noted with the linear wave equation, the first order fRoe scheme has a truncation error dominated by the leading even derivative terms which are dissipative. This combined with the added numerical dissipation due to the Roe-averaged variables results in a less than desirable solution.

The next-best solution was produced by the third-order oRoe scheme. All gradients of density were captured more sharply than the first-order scheme, especially at the left side of the expansion wave as shown in Figure 4.6. Velocity gradients were also better resolved at both the left and right sides as shown in Figure 4.6. Looking in detail at the shock capture in Figure 4.7, the oRoe scheme reduced the width to 9 points for the $\Delta x/L = 0.025$ case. All of these improvements came from the fact that the scheme is using the MUSCL variable extrapolation scheme to improve the overall accuracy. While a limiter was used, and hence the local order of accuracy is only first order at the discontinuities, the overall result is a better match to the exact solution than the fRoe case.

Finally, the best solution was produced by the compact-upwind cRoe scheme. Again, improvements at all gradients were made. As shown in Figures 4.5 and 4.6, the expansion wave with the cRoe solution was very close to the Riemann solution, while the contact

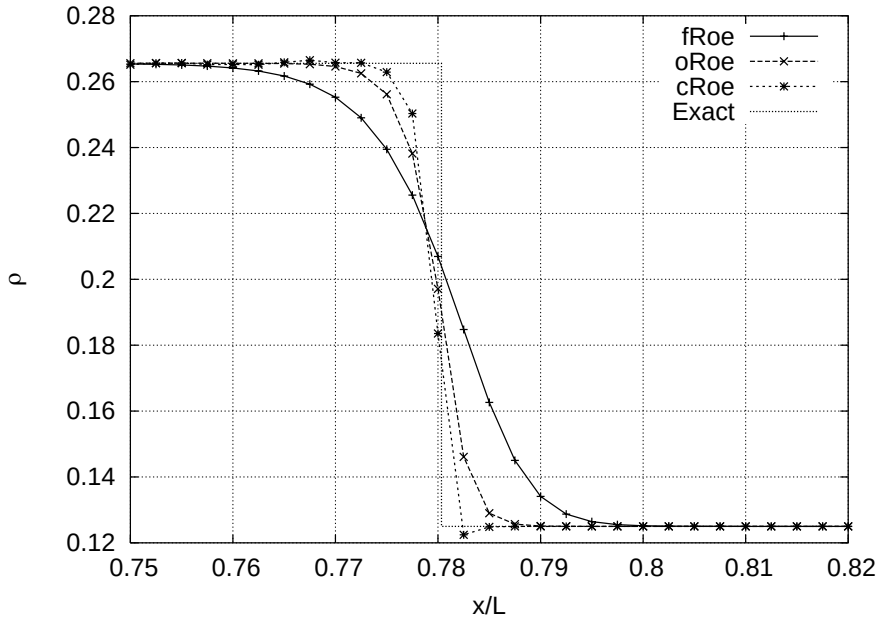

Figure 4.7: Detail of Shock Capture of Roe Method, Density

surface was sharp. The shock capture, shown in Figure 4.7, was further reduced to 5 points for the $\Delta x/L = 0.025$ case. Once again the improvements are most likely due to the higher-order variable interpolation and the use of the compact differencing. It is important to note that the cC compact scheme could not be used on this problem because of stability issues, but the cRoe scheme worked well and showed no stability problems. The only difference between these two schemes is that the cC scheme uses exact fluxes while the cRoe scheme uses Roe-averaged fluxes. The results shows that the Roe fluxes add enough numerical dissipation to eliminate the non-physical behavior of the compact difference method and produce a stable solution.

4.2.5 Accuracy of the cRoe Solution Applied to the 1D Shock Tube. To verify that Equation 3.43 holds true (that the order of a compact formulation using Roe fluxes will have the same order accuracy as the variables at the left and right states) two methods were compared: the third-order oRoe scheme, and a "Compact oRoe" scheme using Equation 1.5 with Roe-averaged fluxes on the right-hand side. Figure 4.8 shows the overall density

distribution and the shock detail for these two methods. It is clear that there is little to no variation in the results of the two schemes. Additionally, the same comparison was made with the first-order Roe scheme and eqaution 1.5 with similar results. This result verifies that the compact formulation of Equation 1.5 will only produce $\partial\hat{F}/\partial x$ terms of same or lesser order than the order of $\hat{F}$ that is used in the right-hand side and that a fourth-order variable interpolation is needed to create a global fourth-order scheme.

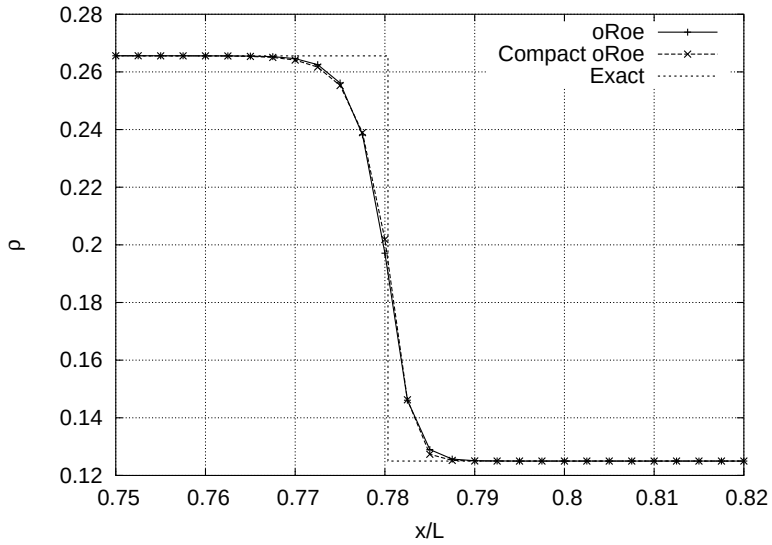

Figure 4.8: Detail of Normal Shock in Comparison of Solutions to 1D Shock Tube Problem at $t = 0.16$.

4.2.6 Variation of the cRoe κ Parameter in the 1D shock tube. There was a large variation in the results of the cRoe scheme when the κ switching parameter was adjusted. κ is a weighting factor which allows the compact interpolant to change bias. In effect it tells the method when the solution is non-smooth and when the stencil should be biased one direction or another. When κ is too high the stencil switches too easily and unnecessary upwinding can occur. When κ is zero the solution reverts back to a central-difference scheme which is unstable across discontinuities. Variation of κ away from the optimal point resulted in oscillations in both the smooth and non-smooth regions of the flow. Deng [3] suggested that $\kappa = 0.5$ was a good all-around value, but the best results were seen with $\kappa = 0.3$. The

results for the density profile around the contact surface with variations in κ can be seen in Figure 4.9. There was a small amount of overshoot (oscillation) seen in the velocity across the shock wave which could not be removed for any value of κ.

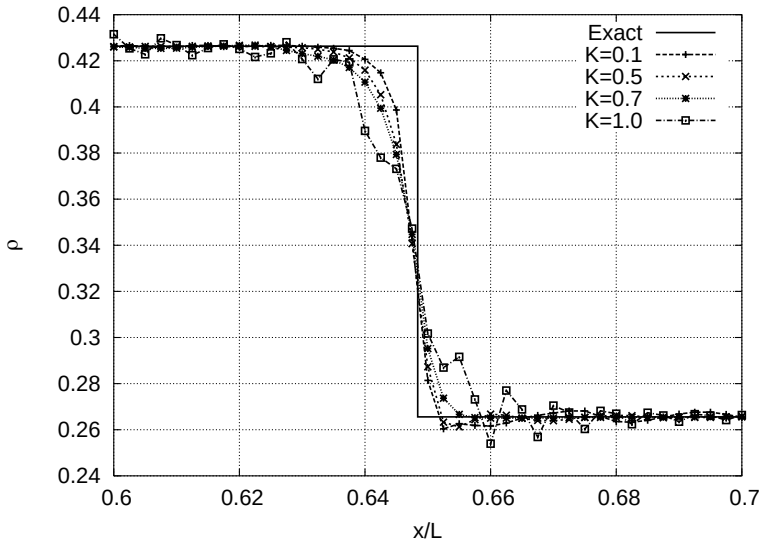

Figure 4.9: Variation in κ Parameter for 1D Shock Tube Problem, Detail of Contact Surface Discontinuity

Deng [3] also suggests that these oscillations are caused by the collision of the characteristics across the discontinuities and that they can be eliminated by performing the variable interpolations on the characteristic variables. The characteristic variables are one level below the primitive variables and are the information that are carried along the characteristics in a hyperbolic solution. Solving on the characteristic level would be very computationally expensive and was deemed unnecessary for the problems considered in this work.

4.2.7 Consistency of the 1D cRoe Scheme. As previously stated, any numerical discretization of a PDE is an approximation and has an associated truncation error term. The scheme is said to be consistent if the error between the PDE and the approximation vanishes as the mesh is refined, i.e. $\Delta x \to 0$. Refining the mesh to this point should make the truncation error vanish. If the scheme is not consistent it is not a useful scheme, as it is not an accurate approximation to the governing equation. The general compact scheme can be readily proven to be consistent through the substitution of TSEs. The compact Roe scheme is more difficult to prove due to the complexity of solving in terms of the Roe averaged variables, and there consistency is examined numerically.

Figure 4.10a shows the results of the cRoe solution near the shock as the grid is refined from $\Delta x/L =$ 5.0E-03 to $x/L =$ 3.125E-04. As the mesh is refined the shock is captured in fewer and fewer cells and the steepness of the shock increases towards the theoretical value. It is apparent from these results that the scheme is consistent as the solution approaches the exact solution rapidly as the mesh is refined. Since the scheme appears consistent it is a valid approximation to the governing equations and should be further investigated.

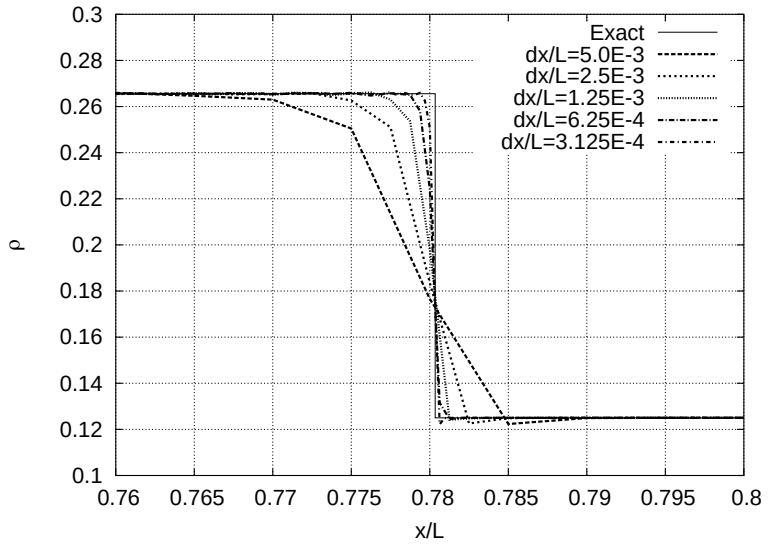

Figure 4.10: cRoe Solution Consistancy to 1D Shock Tube Problem

4.3 2D Shock Tube

Up to this point, all of the results have been previously completed by other parties, and have been duplicated here to ensure repeatability of the solution methods. The next step in investigating the fourth-order cRoe scheme was to extend it to two-dimensions and repeat the shock tube problem.

4.3.1 Problem Description and Setup Conditions. In two-dimensions, the shock tube problem is very similar to the one-dimensional case. Since the initial conditions are only a function of one-dimension, the flow will be uniform in the second dimension and the results will be the same as the one-dimensional case.

Two-dimensional domains with $\Delta x/L$ varied from $5.0E$-03 to $1.25E$-03 were constructed. The domains were of a length of L and a height of $10\Delta x$, and initialized with the same conditions along the length as shown in Table 4.2.3, and constant along the height. The same time steps and total solution time as before were used for the two-dimensional case.

4.3.2 2D Shock Tube Results. Results for the overall density distribution for the two-dimensional shock tube case can be seen in Figure 4.11. Comparing this plot with the one-dimensional results in Figure 4.5, it can be seen that the two-dimensional results agree well. All of the same relevant flow features are present.

4.3.3 Consistency of the 2D cRoe scheme. Again the consistency of the scheme was verified by refining the mesh, and once again the numerical solution approached the exact solution, as shown in Figure 4.12. It was expected that the solution would be consistent in two dimensions, since it was consistent in one dimension, but this result verified that the method was properly implemented into the two-dimensional solver.

4.3.4 Variation of the cRoe κ Parameter in the 2D Shock Tube. Now that the cRoe solution was shown to be a consistent solution in two dimensions, the influence of the κ switching parameter was re-checked. Figure 4.13b shows the results as κ is varied from 0.1 to 0.7. When $\kappa = 0$ the scheme reverts to a fourth order central scheme and becomes unstable. Genearally speaking, the lower the value of κ the better the discontinuities were

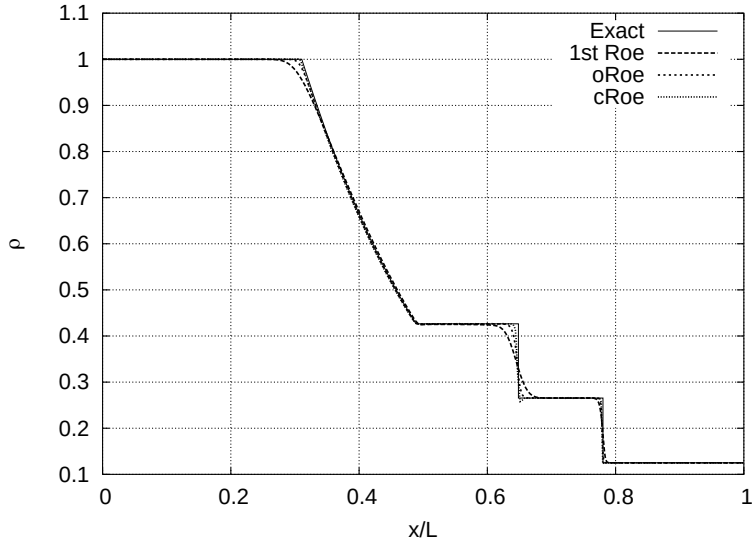

Figure 4.11: Comparison of Density Distribution in 2D Shock Tube Problem at $t = 0.16$.

captured, while the higher the value of κ the more oscillations were seen in smooth regions of the flow. For very low values of κ ($\kappa < 0.1$) there were some oscillations seen near the discontinuities. The results are similar to those seen in the one-dimensional results, most likely due to the fact as κ approaches one the solution is more prone to switching the bias of the interpolant stencil. The more it switches the more likely it will upwind incorrectly and introduce non-physical behavior. It is interesting to note that even when there is error introduced due to this switching, the Roe scheme introduces enough numerical dissipation to maintain stability. A value of $\kappa = 0.3$ was chosen to best balance the capture of the discontinuities and maintain non-oscillatory behavior in the smooth regions.

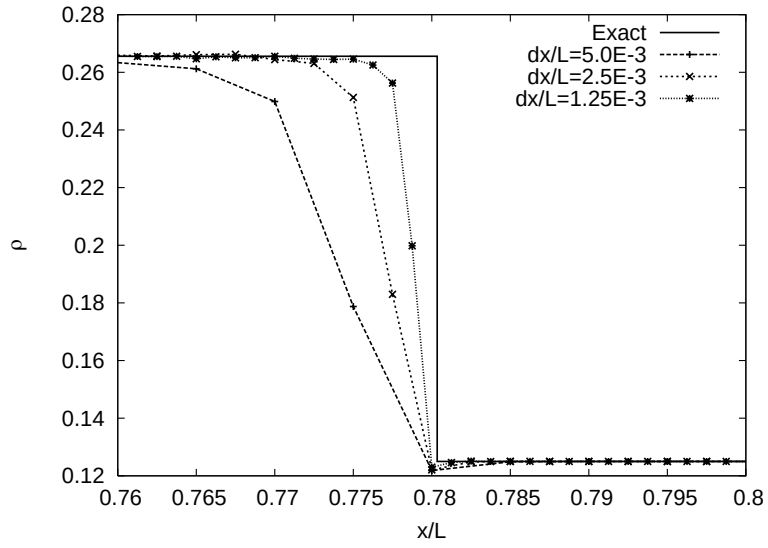

Figure 4.12: cRoe Solution Consistancy to 2D Shock Tube Problem

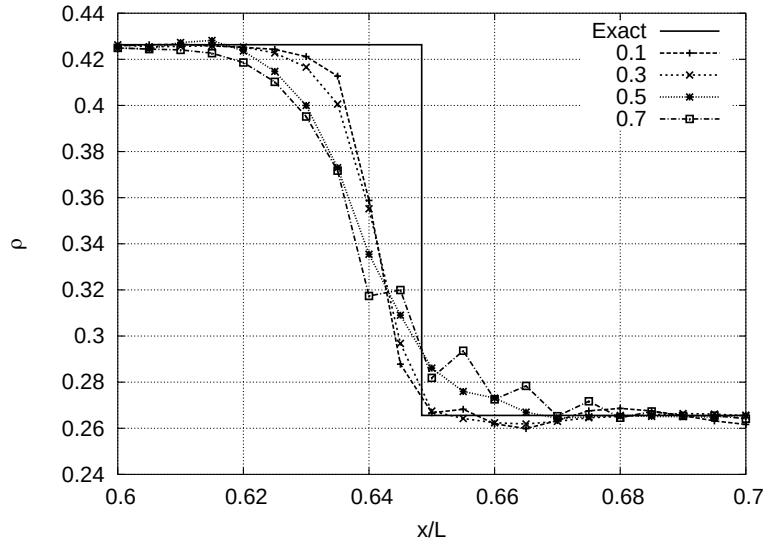

Figure 4.13: Variation in κ Parameter for 2D Shock Tube Problem, Detail of Contact Surface Discontinuity

4.4 Advection of a Vorticial Structure on a Rectilinear Mesh

The accuracy of a numerical approximation is determined by the order of the leading truncation error term. For a scheme that is order n in space, as the grid is refined the truncation error should diminish as Δx^n. For example, the theoretical error of a second order solution should decrease by one-fourth as the grid is refined with twice as many points. If the variation of grid spacing is plotted against the solution error on a log-log plot, the resulting line should have a slope equal to the order of accuracy. This measured order of accuracy should be near the formal order of the scheme, i.e. near the order of the leading truncation error term, but could vary due to other higher-order truncation error term effects.

To measure the order of accuracy of the cRoe scheme a convecting vortex in an otherwise uniform flow was investigated. This problem measures the ability of a numerical simulation to accurately advect vortical structures similar to those found in direct and large-eddy simulations (LES/DNS) [15]. Since higher-order methods are often used in LES/DNS simulations the usefulness of the cRoe method can be shown. Additionally, the problem has a known exact solution at any point in time with which the numerical results can be compared and a formal order of accuracy determination can be made.

4.4.1 Problem Description. The vortex chosen has a central core of vorticity with the same sign as the vortex strength surrounded by a region of vorticity of the opposite sign. This results in a vortical structure which has a total circulation of zero. The initial condition was created by imposing a vortex of strength C at a location (x_c, y_c) and satisfying the following relations [24]:

$$u = u_\infty - \frac{C(y-y_c)}{R^2}\ exp(\frac{-r^2}{2})\ , \quad v = \frac{C(x-x_c)}{R^2}\ exp(\frac{-r^2}{2})$$
$$p_\infty - p = \frac{\rho C^2}{2R^2}\ exp(-r^2)\ , \qquad r^2 = \frac{(x-x_c)^2+(y-y_c)^2}{R^2}$$

where u, v, p and R denote the Cartisian velocity components, static pressure, and vortex core radius. The vortex has maximum vorticity at the center which decreases to a minimum at twice the core radius. The vorticity then decreases in magnitude to zero as x increases. The pressure distribution was obtained by integrating $\partial p/\partial r = \rho u_\theta^2/r$ about the vortex center [24].

4.4.2 Exact Solution to the Vortex Problem. In the absence of viscous dissipation the overall original vortex structure should remain unchanged in time transported a distance $x = U_\infty \Delta t$. All grids and number of iterations were chosen such that the vortex traveled five complete trips through the domain, ending up in the same place that it started. It is important to note that the error in the solutions have two major portions: a phase shift due to the slowing of the vortex and a distortion due to dissipation and dispersion. The phase shift results in the vortex not traveling quite as far as it should have in theory through the domain, while the distortion is due to errors in the solution method itself. To be consistent all solution results are measured against the same theoretical velocity distributions regardless of where the actual solution ended up.

4.4.3 Setup Conditions. The nondimensional vortex strength parameter $C/(u_\infty R)$ was set at 0.02 to match previous work by Visbal and Gaitonde [24] . Constant density was assumed initially as Gaitonde suggested that the uniform density approximation is suitable for most test cases but could be calculated using constant enthalpy for stronger vortices.

The solution was applied to uniform, rectilinear grids with various levels of resolution from $\Delta x/R$=$\Delta y/R$=0.6 to 0.1. This range of grid spacing was chosen to both allow for variation in the solution errors and to keep total computational times reasonable.

The non-dimensional time step was reduced to $\Delta t U_\infty/R$=0.002 which results in a Courant-Friedrichs-Lewy (CFL) number of approximatly 0.02 for the finest mesh. It was determined numerically that this time step allowed the solution to be sufficiently time-resolved at the finest grid spacings which would mean it was also time resolved on the coarsest mesh.

For the oRoe solution the minmod flux limiter was removed to allow a global third-order solution. Limiters work by reverting to first order near non-smooth regions. Even when the solution is "mostly smooth" there still is possibility of limiter influence which would degrade the accuracy of the solution. Since the problem is continuous the use of a limiter is unneeded and it was subsequently removed.

4.4.4 Periodic Boundary Condition. Since the vortex is advected by the free-stream flow the grid would have to be made very large or the solution would have to be

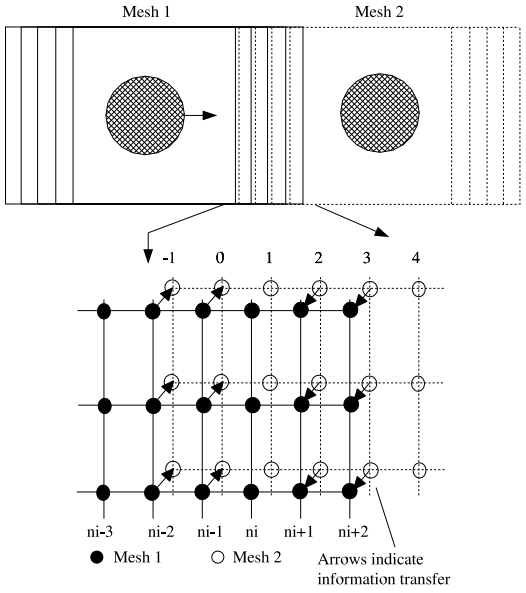

Figure 4.14: Mesh Overlap on Periodic Boundaries

allowed to leave one portion of the domain and re-enter at another. Again, to reduce computational times the latter was chosen and all four sides of the domain were treated with periodic boundary condition. A five point overlap was chosen as shown in Figure 4.14 such that the traveling vortex was allowed to exit one side of the domain and re-enter the opposite side in a cyclic manner. Likewise, any velocity perturbations in the top and bottom of the mesh were allowed to exit and re-enter the domain. Visbal and Gaitonde [5] have shown five points are a sufficient overlap to preserve the accuracy of the solution on the periodic boundary and little degradation of the solution occurs.

Mesh dimensions of $-6 \leq x \leq 6$ and $-6 \leq y \leq 6$ were chosen such that at the initial state the velocity at the boundaries of the domain were near machine zero. A smaller domain could have allowed feedback across the domain in every iteration, whereas the larger domain only transmitted information across the boundary when the vortex had traveled across the domain.

The implicit calculation of the convective gradients ($\hat{F}'$ and $\hat{G}'$) and the implicit calculation of the left and right variable states for the cRoe method were modified due to

the periodic boundaries. The implicit matrix was now considered as a full periodic tri-diagonal system where the first and last rows of the left-hand side contain a non-zero term in the last and first column respectively. This resulting system was directly solved using a periodic tri-diagonal solver [10].

4.4.5 Results to the Vortex Problem. Figure 4.15 shows contours of constant vorticity magnitude at $t = 8.0$ for the exact, oRoe, cC, and cRoe methods on the $\Delta x/R = 0.2$ mesh. It is clear that all methods did fairly well preserving the overall velocity distribution near the center of the domain, but all methods suffered towards the outer edges of the vortex. The oRoe method showed a maximum error along planes $\pi/4$ from the coordinate axes consistent with published results [24]. Gaitonde noted that this is due to a bias inherit to the Roe scheme itself and is generally harmless for most solutions [6]. The fourth-order cRoe and the fourth-order cC schemes both show similar results, with slightly better flow preservation than the third-order oRoe scheme. All three methods continued to act consistently as they approached the theoretical value as the mesh was refined.

Figures 4.16, 4.17, and 4.18 show the swirl velocity and vorticity profiles along the $y = 0$ centerline for the oRoe, cC, and cRoe methods respectively. The oRoe method showed the most dissipation error for all values of $\Delta x/R$ with the largest errors on the coarsest mesh. For $\Delta x/R = 0.3$, the resulting peak vorticity magnitude was only 40% of the initial value. This result is contrasted to the cC and cRoe schemes which, on this mesh, recovered 93% and 86%, respectively, of the original peak values. The oRoe scheme also caused a smoothing of the velocity distribution with the peak values diminished and the vortex width broadened, both due to the inherit dissipative nature of the oRoe scheme. It is worth noting that a first-order Roe scheme, similar to the fRoe shown on the shock tube, would have completely dissipated the vortex after one cycle through the domain.

The cC compact method did the best job of the three schemes at preserving the peak velocity values, but was also the most dispersive of the three. For many of the cC test cases shown in Figure 4.17 the solution exhibited a lagging phase error with the vortex slightly shifted to the left of the theoretical location, and more so on the coarsest mesh. There was also a large amount of oscillations at the trailing edge of the vortex, also due to dispersion.

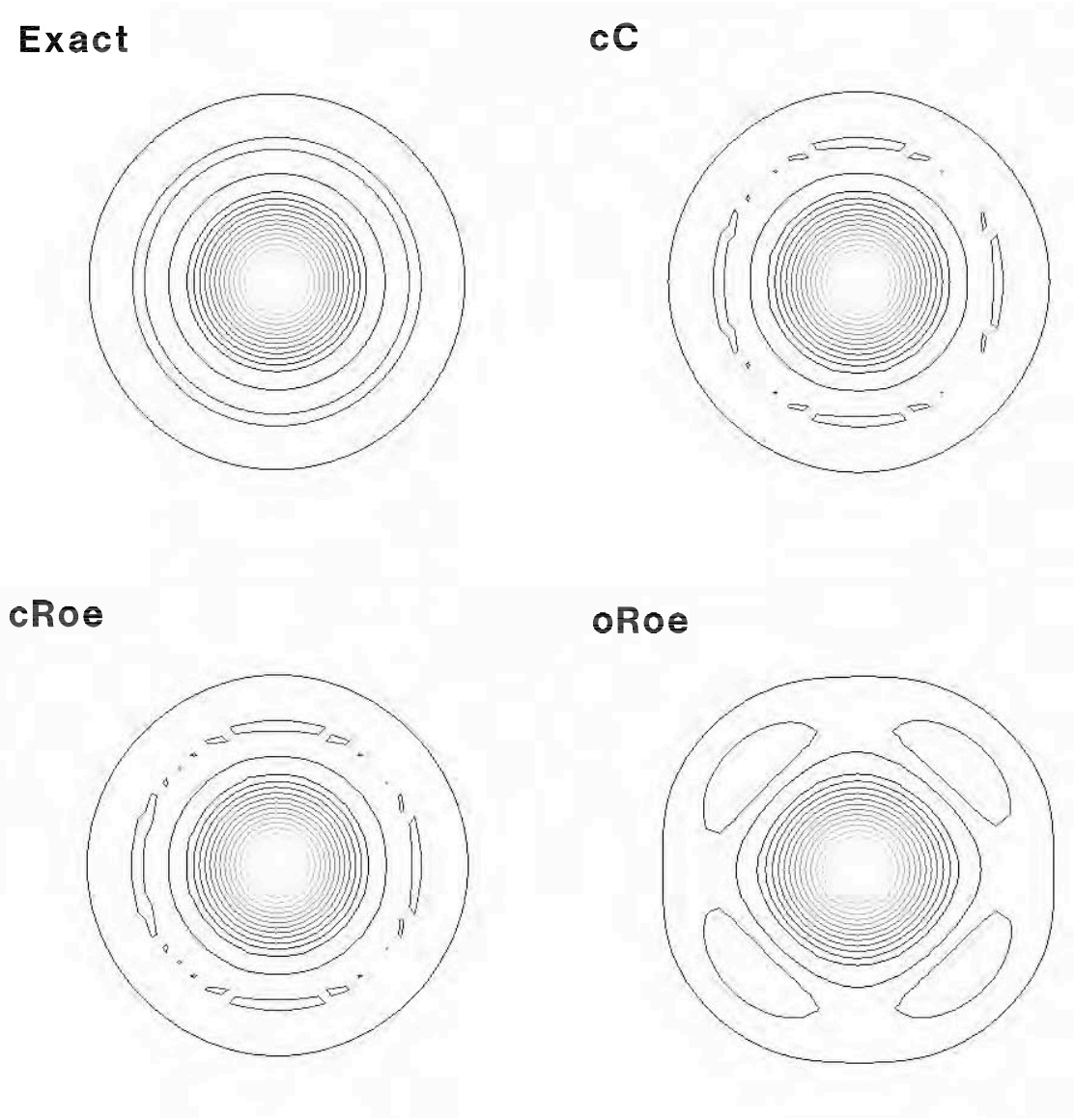

Figure 4.15: Vorticity Profiles of Advecting Vortex at T=30.0, $\Delta x/R$=0.20

As mentioned previously, the fourth-order scheme has a truncation error dominated by an odd-ordered derivative term which produces the dispersion effect.

The cRoe method, (Figure 4.18), exhibited similar results to both the oRoe and cC schemes (Figures 4.16 and 4.17, respectively), most likely since it contains elements of each of them. The cRoe scheme did a better job of preserving peak values of velocity than the oRoe method, but not quite as good a job as the cC compact scheme did. However, the cRoe scheme did not display as much dispersion or phase error as the cC scheme did, most likely due to the added numerical dissipation from the Roe fluxes.

Figures 4.19, 4.20, and 4.21 show the associated error of the oRoe, cC, and cRoe methods respectively, for both swirl velocity and vorticity magnitude along the $y = 0$ centerline. Again, the oRoe method had the largest errors associated for the velocity profile, with errors of nearly an order of magnitude more than the cC and cRoe compact schemes. Overall the cC scheme had the lowest overall absolute errors based on a L_∞ norm, with the cRoe coming in second, and the oRoe last.

The oRoe errors were smoothly distributed across the domain with a shape similar to the associated function. The compact schemes produced errors of a lesser magnitude, but with more variation across the domain, similar to the errors seen in the linear wave equation. Again, this could be attributed to the numerical dissipation of the oRoe scheme and the dispersive nature of the compact difference. The compact schemes do a better job of resolving the high-frequency waves in the solution, whereas the oRoe scheme damps them out. This makes the oRoe scheme slightly more stable and robust than the compact schemes, but also removes small scale information from the flow. If the goal of the solution is to produce a well-behaved, stable result the oRoe scheme would be a good choice. If the goal of the solution is to capture as much of the flow structure as possible, with the possibility of some instabilities, the compact methods would be best.

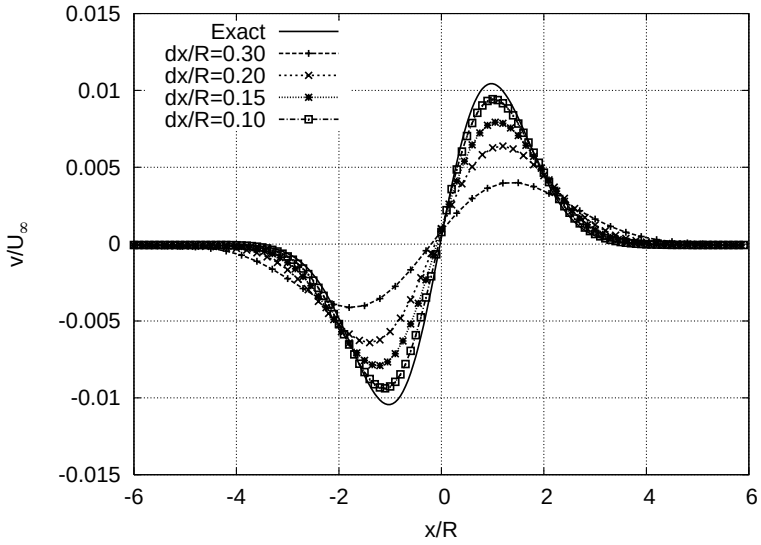

(a) Swirl Velocity

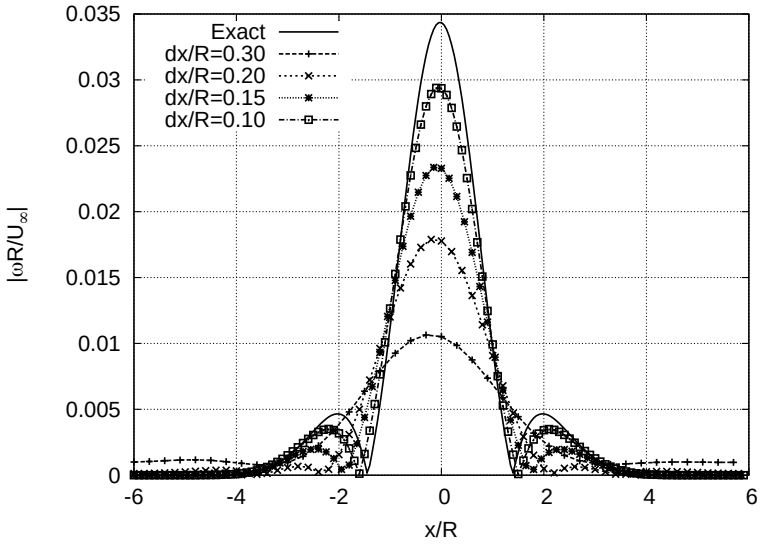

(b) Vorticity Magnitude

Figure 4.16: Comparison of oRoe Solutions to Vortex Problem along centerline after $t = 30$.

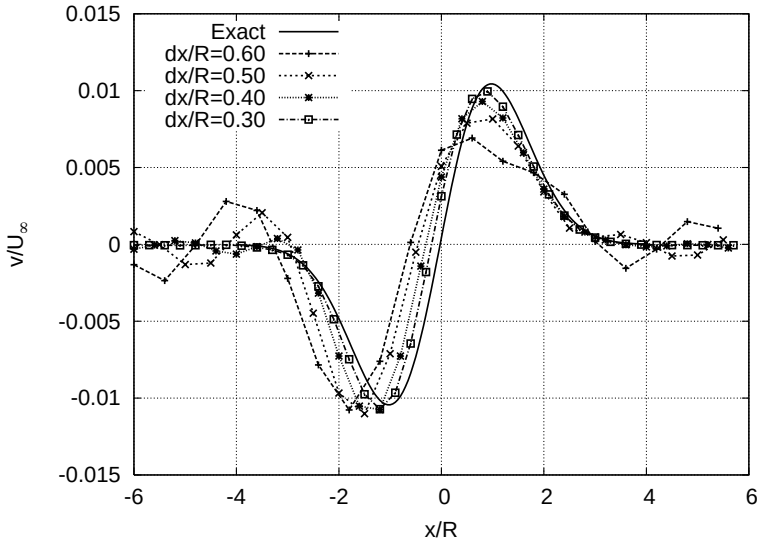

(a) Swirl Velocity

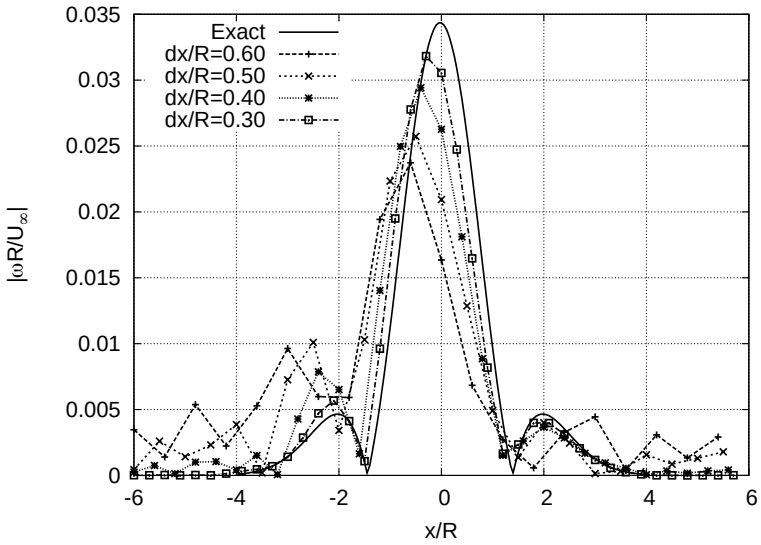

(b) Vorticity Magnitude

Figure 4.17: Comparison of cC Solutions to Vortex Problem along centerline after $t = 30$.

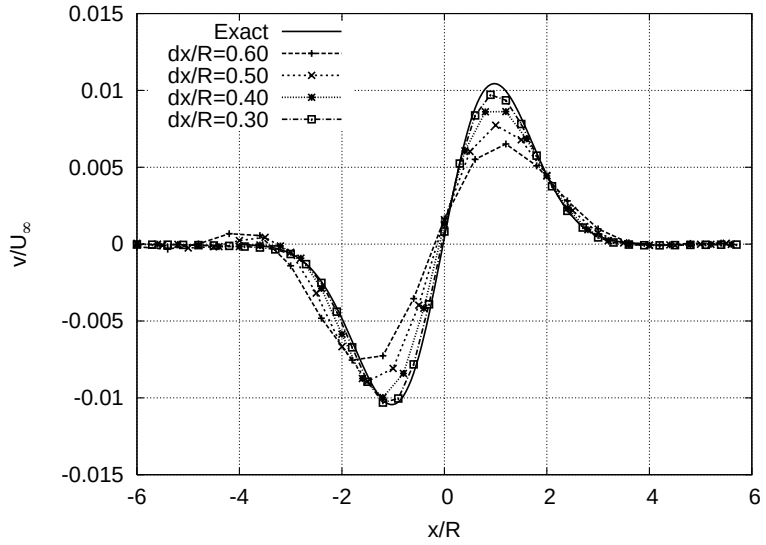

(a) Swirl Velocity

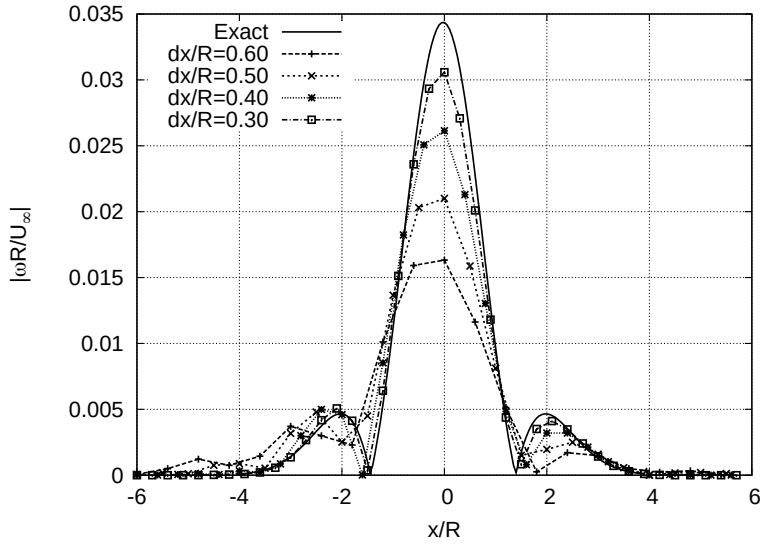

(b) Vorticity Magnitude

Figure 4.18: Comparison of cRoe Solutions to Vortex Problem along centerline after $t = 30$.

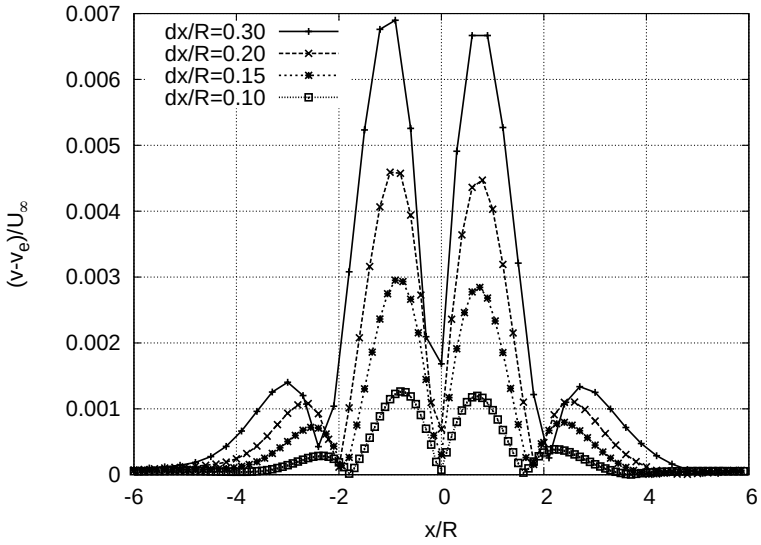

(a) Swirl Velocity Error

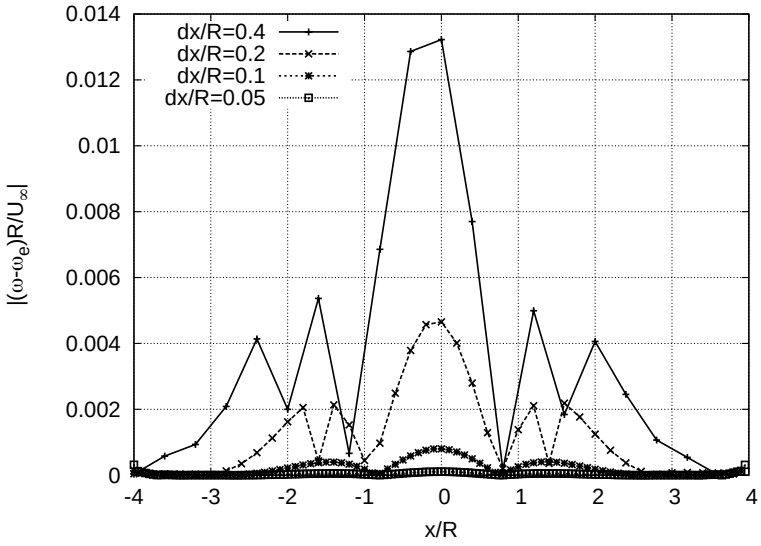

(b) Vorticity Magnitude Error

Figure 4.19: Comparison of Error in oRoe Solutions to Vortex Problem along centerline after $t = 30$.

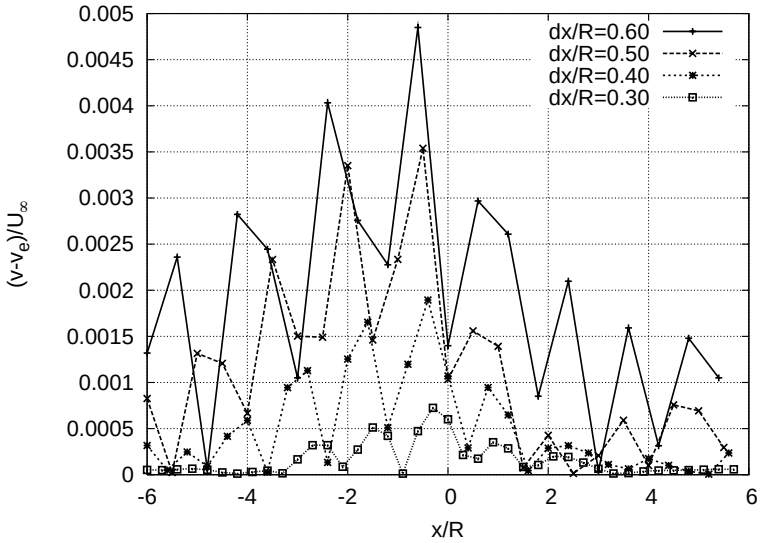

(a) Swirl Velocity Error

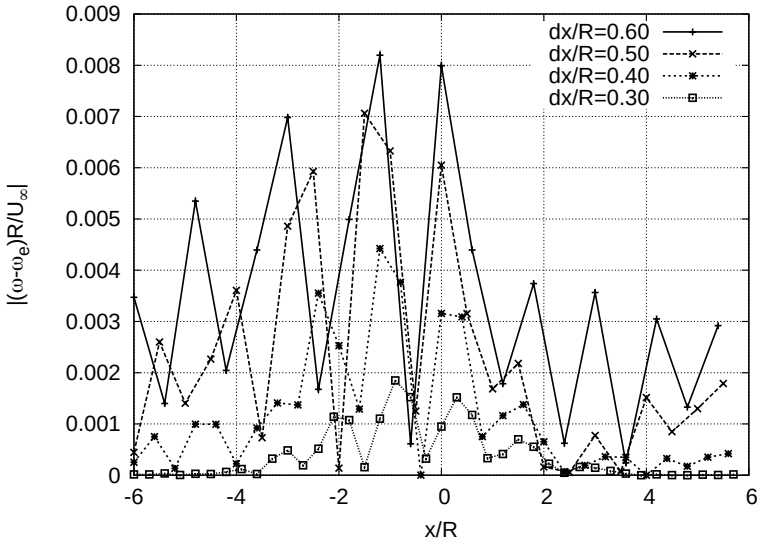

(b) Vorticity Magnitude Error

Figure 4.20: Comparison of Error in cC Solutions to Vortex Problem along centerline after $t = 30$.

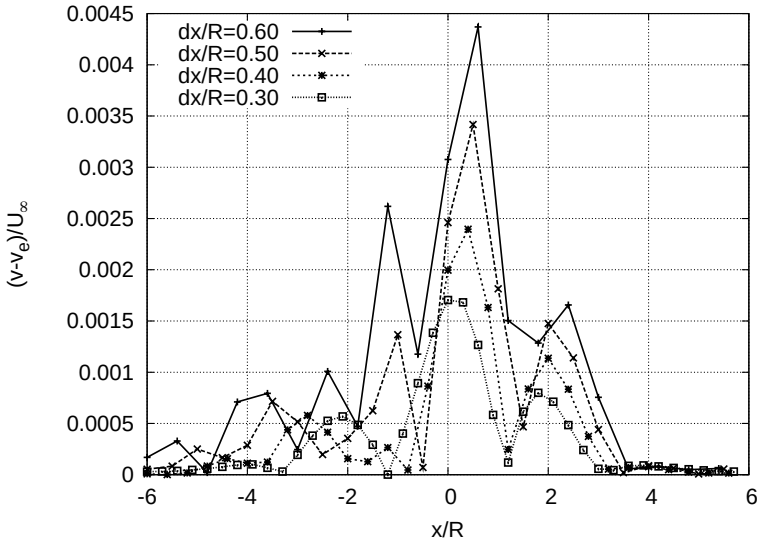

(a) Swirl Velocity Error

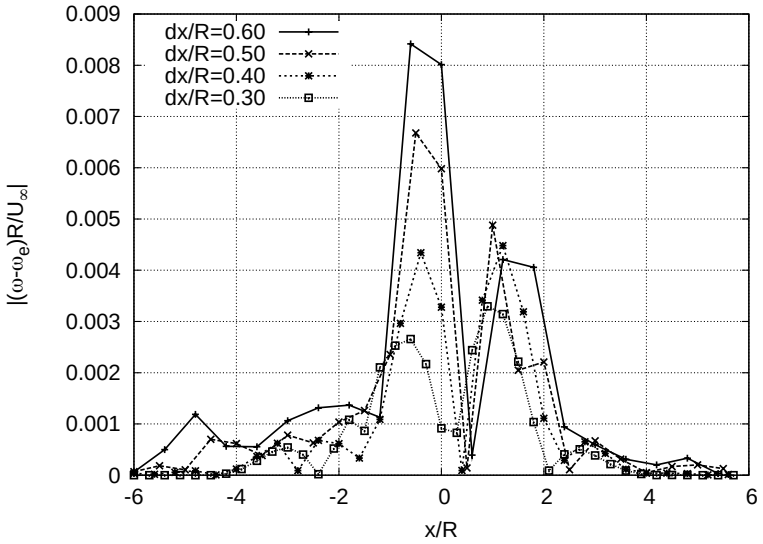

(b) Vorticity Magnitude Error

Figure 4.21: Comparison of Error in cRoe Solutions to Vortex Problem along centerline after $t = 30$.

4.4.6 Order of Accuracy Determination. For the order of accuracy determination, an L_2 norm of the swirl velocity along the $y = 0$ centerline was calculated and plotted against the non-dimensional grid spacing $\Delta x/R$. The swirl velocity was chosen because it is not a derived quantity (like vorticity), the use of which could inadvertently add additional error to the solution. The L_2 norm was chosen as it provided the best match to published results for the third-order oRoe scheme and the fourth-order cC scheme. The computed orders of accuracy based on a least-squares fit of the log of the error versus the log of the grid spacing are presented graphically in Figure 4.22 and numerically Table 4.1.

Table 4.1: Theoretical and Calculated Orders of Accuracy for Various Solution Methods

	oRoe	cC	cRoe
Theoretical	3.0	4.0	4.0
Computed	2.8	3.9	3.4

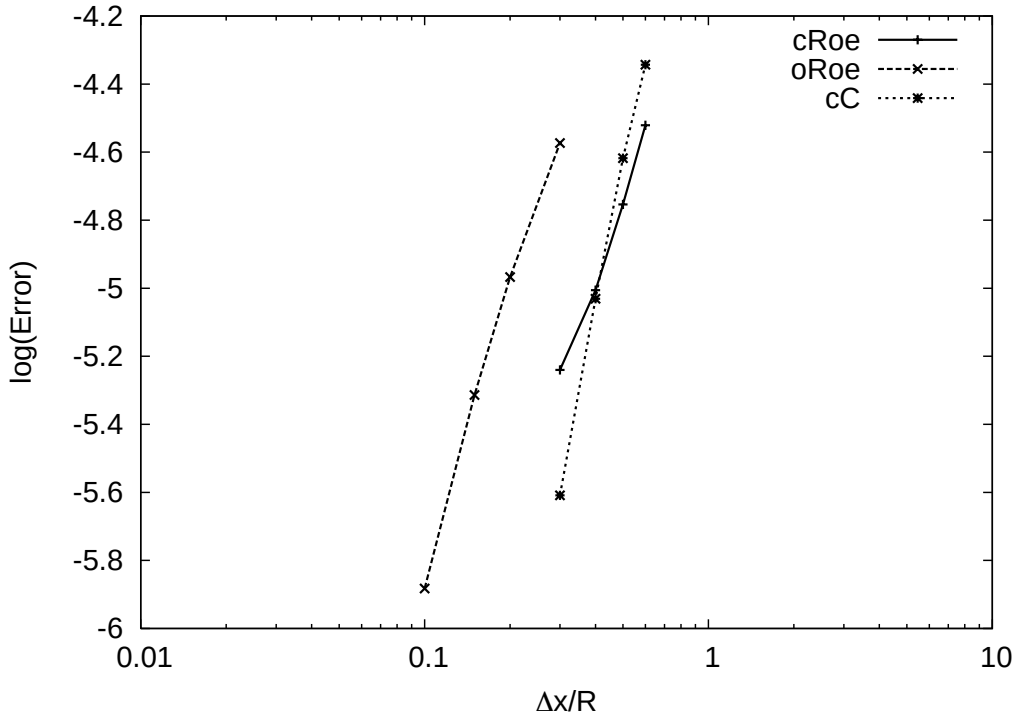

Figure 4.22: Order of Accuracy of Solution Methods

The orders of accuracy of the oRoe method and the cC method were comparable with both the theoretical and published values [24]. The cRoe method was slightly lower than anticipated, as it was expected to be a fourth-order solution. However, when the distinction between order of accuracy and absolute error is made, the cRoe method clearly has a large advantage over the oRoe scheme. For a consistent scheme, order of accuracy says nothing about how close a method is to approximating an exact value, but rather the rate at which the solution approaches the exact value. For the case of the cRoe scheme, while it is not approaching the exact solution at as great a rate as the cC compact scheme, it produced absolute errors comparable to those of the cC scheme and much lower than the oRoe scheme. The fact that the error was comparable with the cC method, but that it could be applied to a discontinuous solution is a very important finding.

While the method presented for determining order of accuracy is theoretically sound, it does have it's pitfalls. For highly accurate schemes there is a delicate balance between producing too good of a solution with a highly machined mesh and producing a very poor solution due to a coarse mesh. The oRoe method was run on more refined meshes than the compact schemes, principally due to this fact. When the compact schemes were run with a mesh spacing less than $\Delta x/R = 0.2$ the error calculations decreased in slope drastically, or leveled-off altogether. Physically what is happening is that at these levels of mesh refinement the compact methods preserve the flow so well that the errors have reached the range of machine zero and cannot be improved upon. The only option for this case is to coarsen the mesh and try to increase the error of the solution. However, when the mesh is coarsened the oRoe method had the opposite problem. The oRoe method was unable to produce a solution on a mesh with spacing greater than $\Delta x/R = 0.4$ due to the magnitude of the error terms. When the mesh is very coarse the solution error behaves very nonlinearly and it is difficult to draw conclusions. The grid with $\Delta x/R = 0.3$ proved to be the point in common which all solution methods worked well. It is this problem of balancing the mesh refinement that causes the orders of accuracy to be slightly different than the theoretical values. These problems are further aggravated by the fact that the advecting vortex is a relatively simple problem. In order to introduce more error for the compact methods, a more difficult problem would be needed. The drawback to attempting a more difficult problem is that they often have less defined exact solutions for comparison. Again, even though the three methods

only shared one common mesh refinement, it is clear that the compact methods produced much lower absolute error than the oRoe method did. This result means that a solution could be run on a coarser mesh with the compact methods than the oRoe method but still have a lower overall absolute error.

4.5 Advection of a Vortical Structure on a Curvilinear Mesh

Thus far two dimensional results have been presented on uniform rectilinear meshes. While these meshes are suitable for analytic investigations, they are not realistic problems. There are not too many "real-world" problems that occur with flow on a uniform rectilinear domain. In order to be useful, a solution must be able to handle variations in the mesh due to stretching and skewing. On a two-dimensional rectilinear mesh the physical domain exactly aligns with the computational domain and the associated grid metrics are either unity or zero. When the metrics are non-zero they can have a great influence on the outcome (and accuracy) of the solution.

4.5.1 Problem Description and Setup Conditions. To understand how the solution methods perform on a smooth but non-orthogoal curvilinear grid a new set of meshes were generated analytically according to [5]:

$$\begin{aligned} x_{i,j} =& x_{min} + \Delta x_o[(i-1) + A_x sin(n_x \pi (j-1)\Delta y_o / L_y + j\phi_x / ii) \\ y_{i,j} =& y_{min} + \Delta y_o[(j-1) + A_y sin(n_y \pi (i-1)\Delta x_o / L_x + j\phi_y / jj) \\ \Delta x_o =& L_x/(ii+1) \\ \Delta y_o =& L_y/(jj+1) \\ & 1 \le i \le ii \\ & 1 \le j \le jj \end{aligned} \tag{4.10}$$

ii and jj denote the number of grid points in the x and y directions, respectively, with $L_x = x_{max} - x_{min}$ and $L_y = y_{max} - y_{min}$. The amplitude, frequency, and phase shift parameters were specified as $A_x = A_y = 0.5$, $n_x = n_y = 4$, and $\phi_x = \phi_y = 0.0$, respectively. The lengths and number of nodes were set such that the average node spacing matched the previous rectilinear results. The resulting mesh has a maximum aspect ratio of 1.8, a ratio of maximum to minimum cell size of 1.84, and a maximum deviation from orthogonality (equi-angle skewness) of 0.42. An example mesh is shown in Figure 4.23.

The three solution methods were used to solve the same advecting vortex problem described by equation 4.10 with the same solution settings and methods. The grid metrics which map the curvilinear domain to the computational domain were computed using a

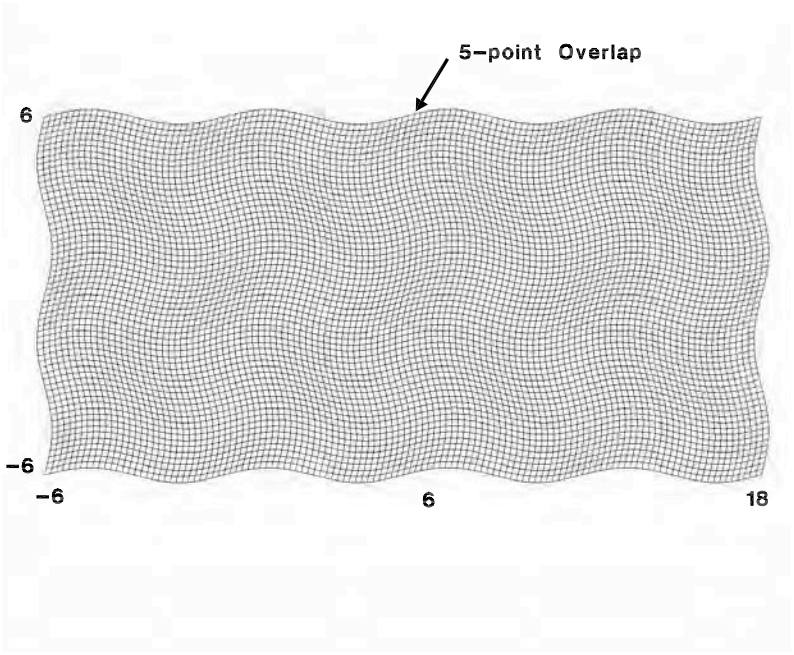

Figure 4.23: $\Delta x/R = 0.2$ Curvilinear Mesh with 5-point Overlap

fourth-order compact difference method similar to Equation 3.3 to ensure a global higher-order accurate solution.

4.5.2 Curvilinear Vortex Advection Results. Figures 4.24, 4.25, and 4.26 show the centerline swirl velcocity and vorticity magnitudes along $y = 0$ for the oRoe, cC, and cRoe methods, respectively. Again, as somewhat expected, the oRoe scheme did the worst with a great deal of dissipation in all test cases. After five trips through the domain the oRoe method had retained less than 40% of the initial signal. The cC and cRoe methods did much better than the oRoe method, but still had greater dissipation and dispersion errors than the rectilinear results. This was an anticipated result, as the curvilinear mesh is a more difficult problem to solve and should introduce more error into the solution. As seen in other problems, this error is manifest mainly as dissipation in the oRoe method and as dispersion in the compact methods.

When the cC and cRoe methods are compared on Figures 4.25 and 4.26, respectively, the cRoe appeared to produce better results on the curvilinear mesh than the straight compact method did. The cC method had a large amount of oscillations on the middle

$\Delta x/R = 0.3$ mesh, while the cRoe scheme was relatively nonoscillatory. This could be attributed to the added numerical dissipation the Roe scheme adds to the solution, removing the oscillations.

Figures 4.27, 4.28, and 4.29 show the error distribution for swirl velocity and vorticity magnitude for the oRoe, cC, and cRoe methods respectively along the $y = 0$ centerline. Results were similar to those of the rectilinear mesh for all schemes, except the magnitudes of error nearly doubled. While the L_∞ norms for the cC solutions were almost always lower than the cRoe solutions, the cRoe solution had much less dispersion error and seemed to do a better overall job of preserving the initial conditions.

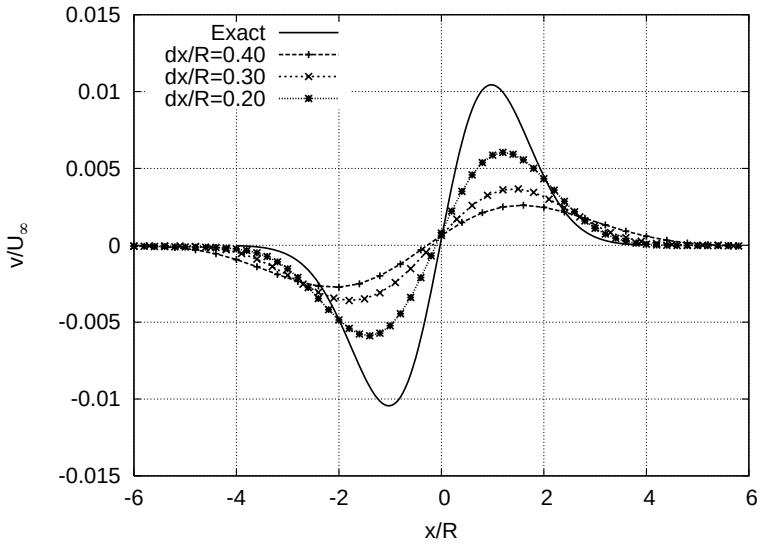

(a) Swirl Velocity

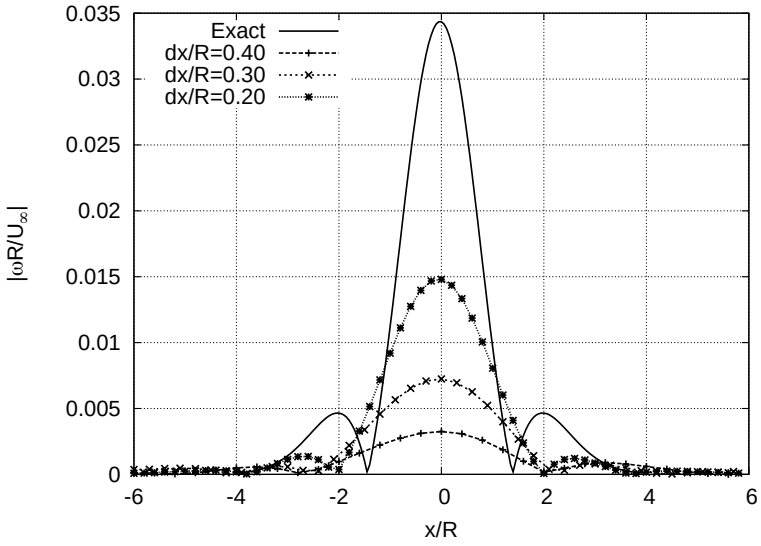

(b) Vorticity Magnitude

Figure 4.24: Comparison of oRoe Solutions to Vortex Problem on a Curvilinear Mesh Along Centerline After $t = 30$.

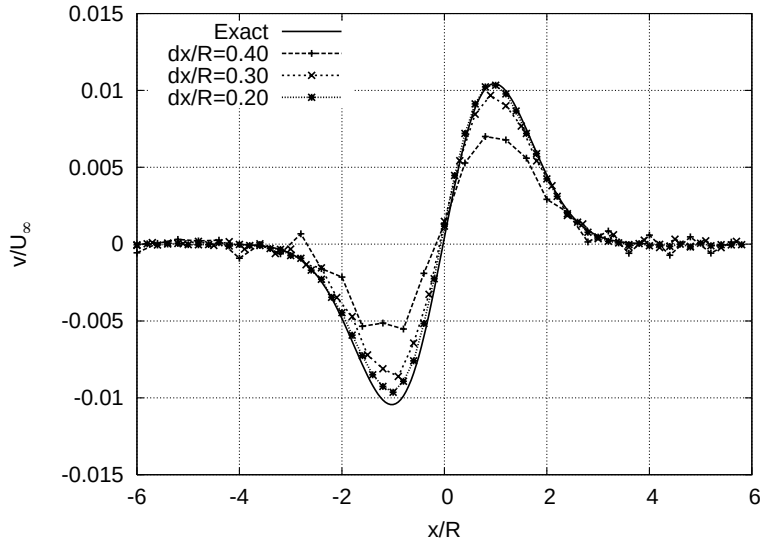

(a) Swirl Velocity

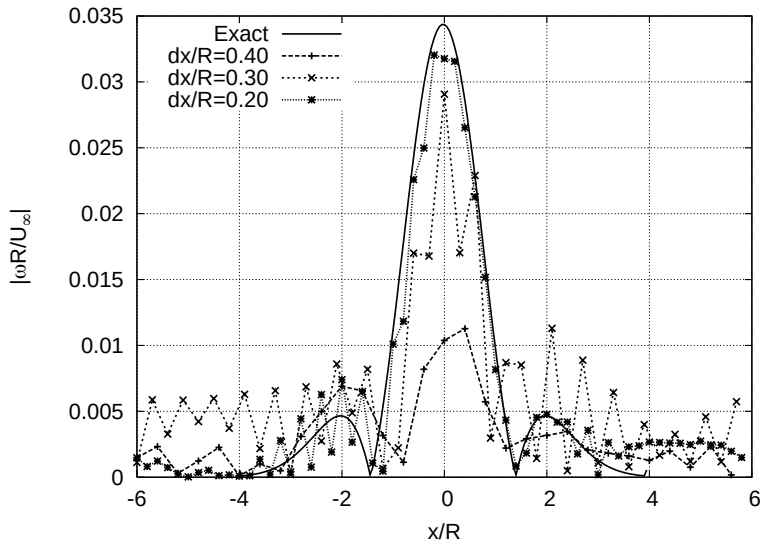

(b) Vorticity Magnitude

Figure 4.25: Comparison of cC Solutions to Vortex Problem on a Curvilinear Mesh Along Centerline After $t = 30$.

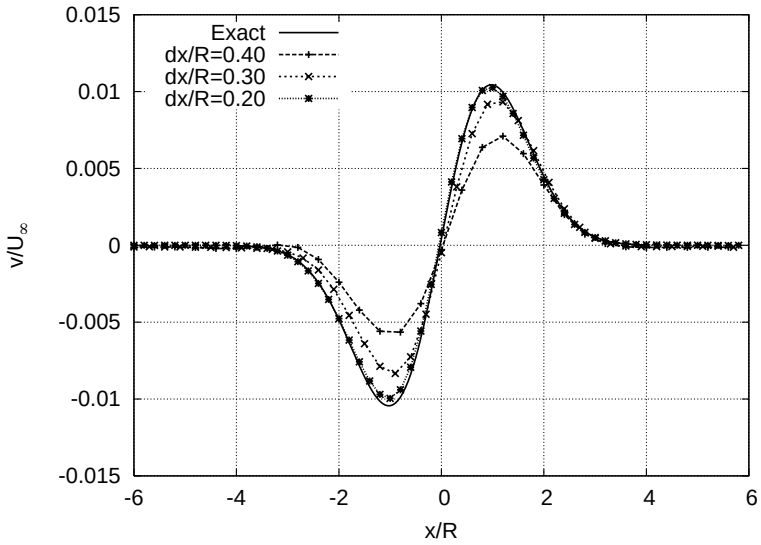

(a) Swirl Velocity

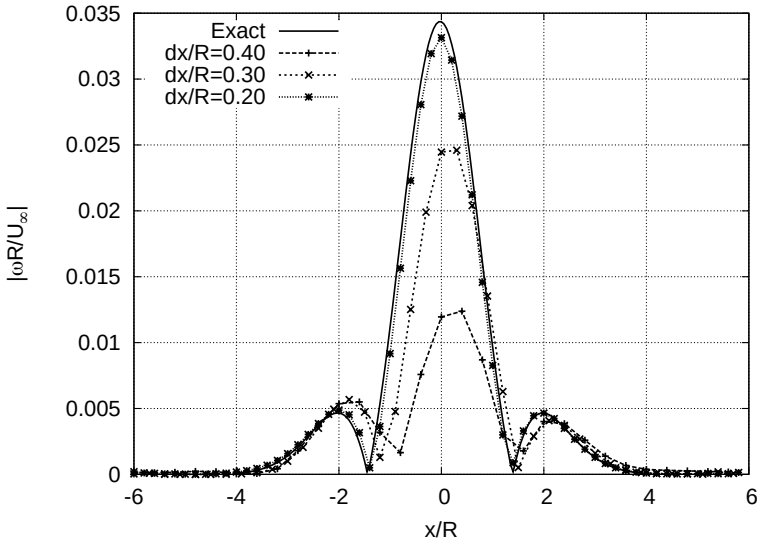

(b) Vorticity Magnitude

Figure 4.26: Comparison of cRoe Solutions to Vortex Problem on a Curvilinear Mesh Along Centerline After $t = 30$.

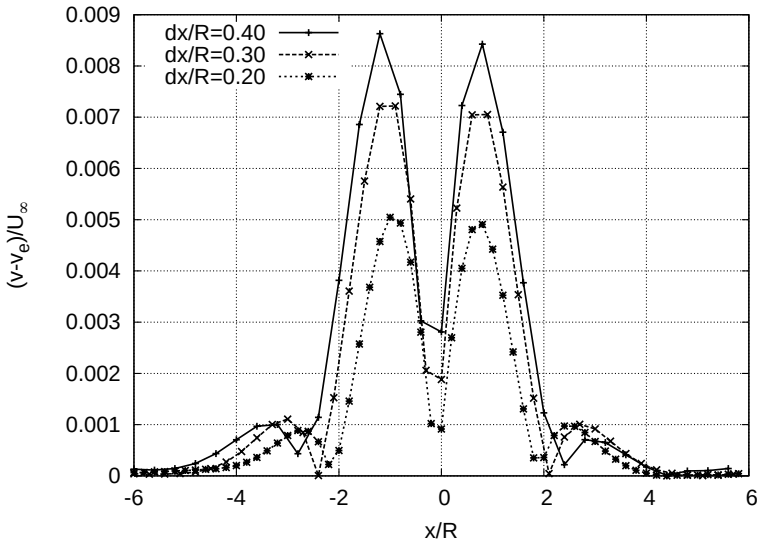

(a) Swirl Velocity Error

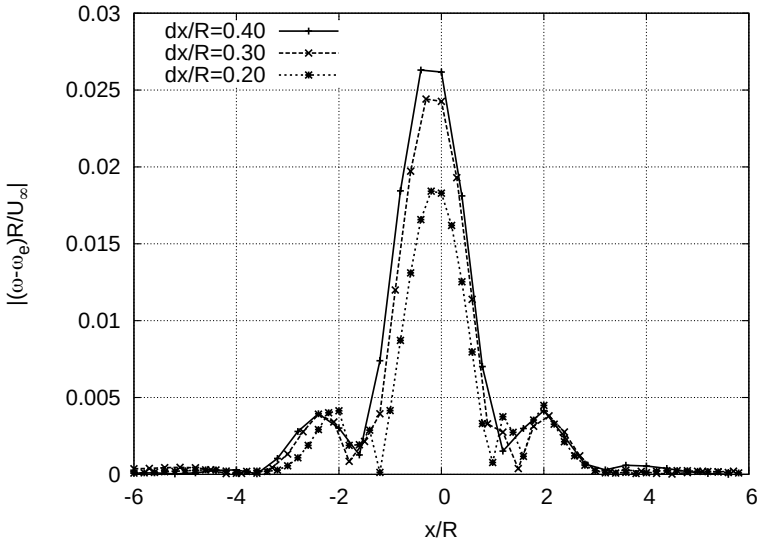

(b) Vorticity Magnitude Error

Figure 4.27: Comparison of Error in oRoe Solutions to Vortex Problem on a Curvilinear Mesh Along Centerline After $t = 30$.

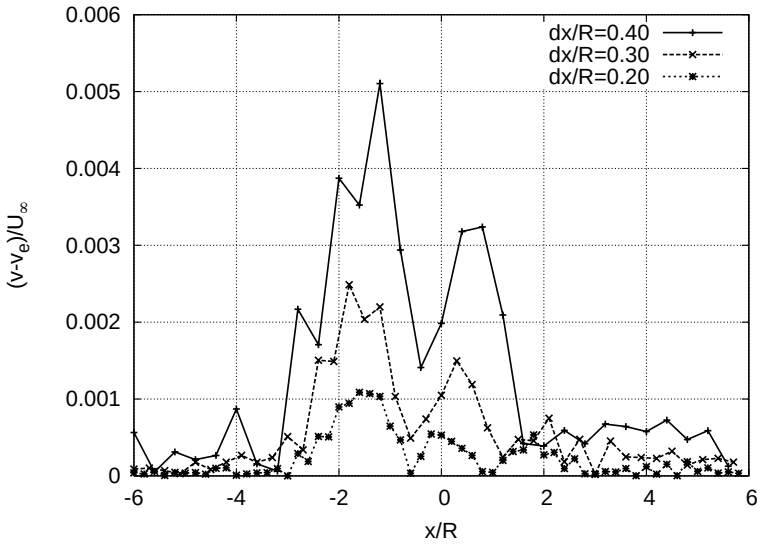

(a) Swirl Velocity Error

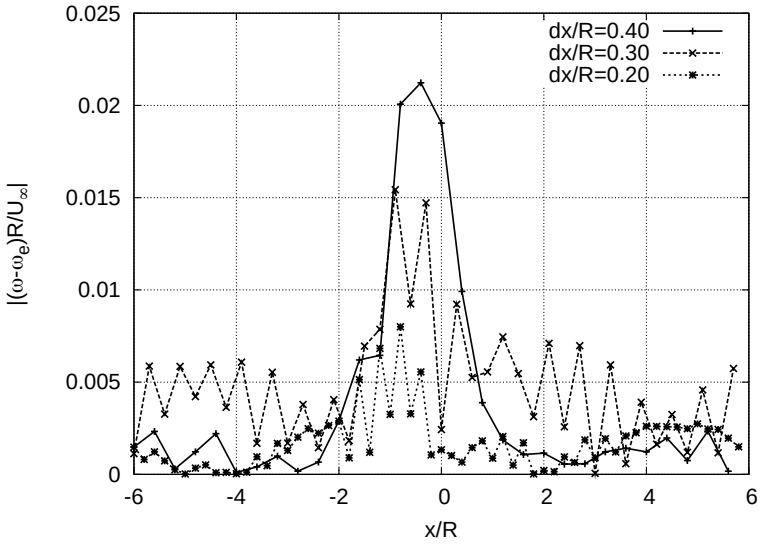

(b) Vorticity Magnitude Error

Figure 4.28: Comparison of Error in cC Solutions to Vortex Problem on a Curvilinear Mesh Along Centerline After $t = 30$.

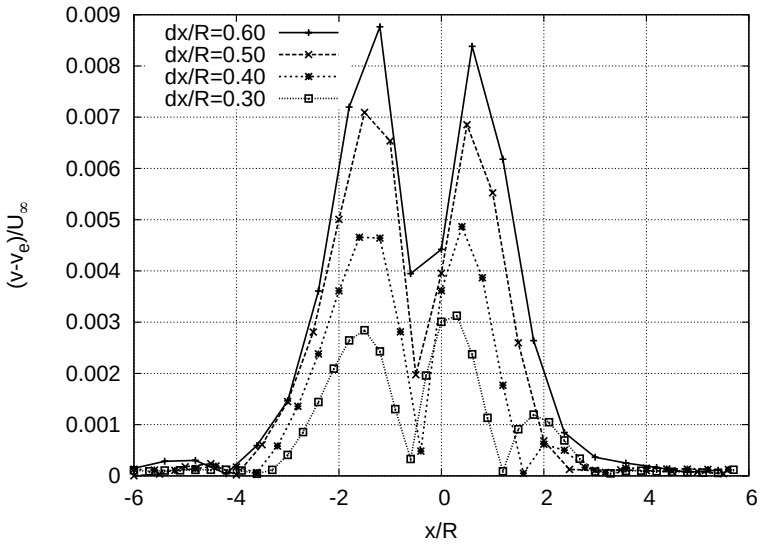

(a) Swirl Velocity Error

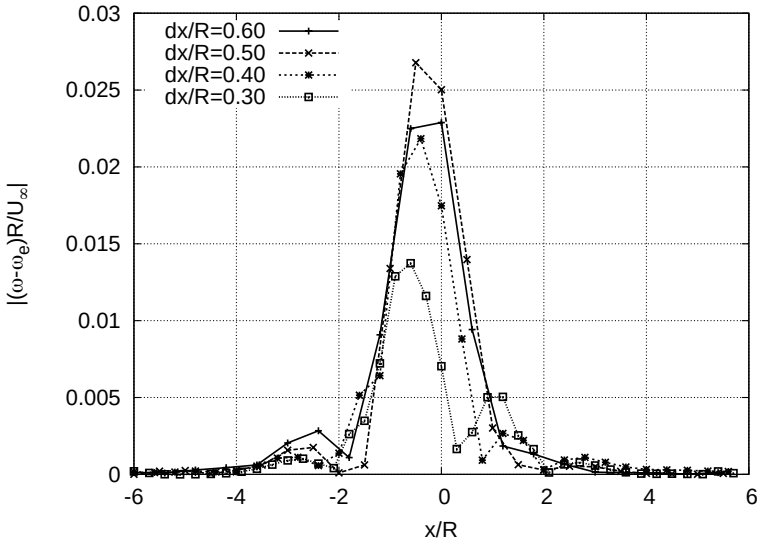

(b) Vorticity Magnitude Error

Figure 4.29: Comparison of Error in cRoe Solutions to Vortex Problem on a Curvilinear Mesh Along Centerline After $t = 30$.

4.5.3 Order of Accuracy Determination on Curvilinear Mesh. Again, the order of accuracy was determined with a least-squares fit to the error and grid spacing data. The results of these calulcations are shown in table 4.2.

Table 4.2: Theoretical and Calculated Orders of Accuracy for Various Solution Methods on a Curvilinear Mesh

	oRoe	cC	cRoe
Theoretical	3.0	4.0	4.0
Computed	2.4	3.3	3.8

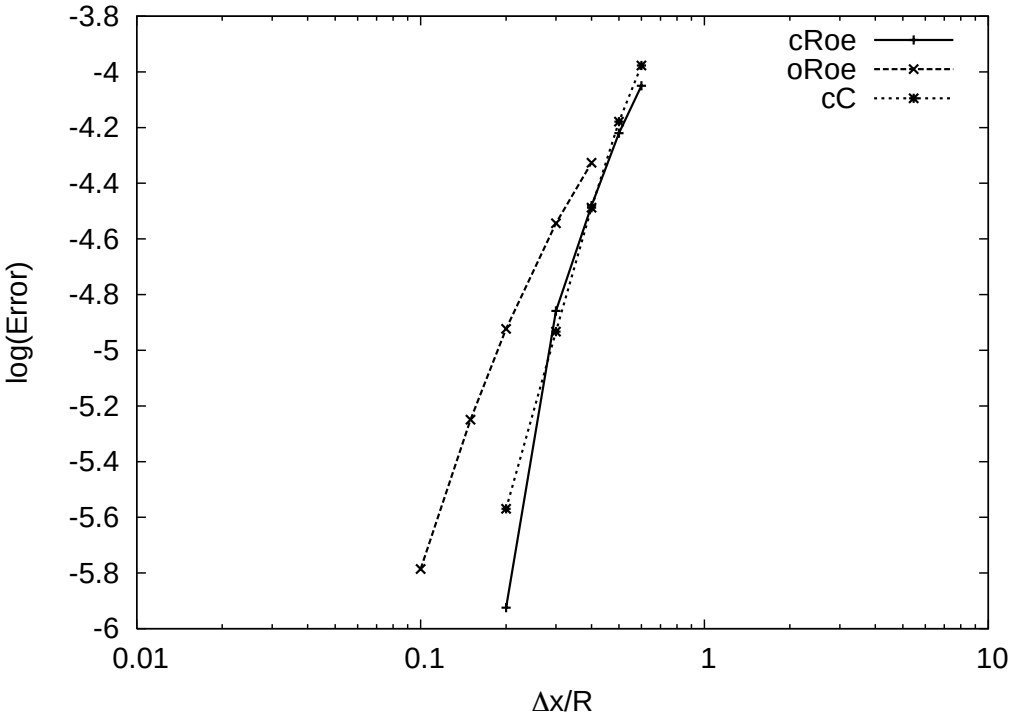

Figure 4.30: Order of Accuracy of Solution Methods on a Curvilinear Mesh

The order accuracy of the oRoe and cC methods decreased slightly, which was expected and in accordance with published results [24]. All of the methods investigated are derived using some sort of difference equation, either a finite difference or a compact difference. Both of these difference methods assume a constant node spacing Δx in their derivation using

Taylor series expansions. On the rectilinear mesh this is correct, but it is not true on the curvilinear mesh. The cell metrics take some of this non-uniformity into account, but they do not eliminate its effect all together. Additionally, the order of accuracy determination assumes a constant node spacing, and that all cells change at the same rate as the mesh is refined. For a rectilinear mesh this is also correct, but in a mesh with skewed cells the spacing is non-uniform and cell sizes will change at different rates. However, the results of an order of accuracy determination on a curvilinear mesh is still interesting for it shows the utility of a solution on a non-ideal mesh. Since most physical geometries require non-ideal grids, it is a worthwhile experiment.

The surprise for this experiment was the fact that the slope of the cRoe error curve increased over that of the rectilinear results. The same cautionary statement applies to the curvilinear results that did to the rectilinear results: the order of accuracy is only a measure of the rate of change of error, while the absolute error is generally the more useful result. The order of accuracy dictates the rate at which the solution approaches the exact value, while the absolute error is the difference between the approximation and the exact value. If the absolute error is already low, the rate at which it approaches the exact solution is not as important. For the curvilinear meshes the cRoe scheme constantly produced results with less absolute error than the oRoe scheme, and sometimes the cC scheme. The fact that the cRoe scheme absolute error is comparable to the cC scheme and it can be used on discontinuous solutions is a very promising result.

4.5.4 Variation of cRoe κ Parameter in Vortex Problem. As seen with the shock tube problem, the κ weighting factor had an influence on the performance of the scheme. One can recall that this κ factor is a switch to tell the compact adaptive interpolation which direction to go. A value of $\kappa = 0$ gives the interpolant a fixed central stencil, while $\kappa > 0$ allows the interpolant to switch directions. Larger values of κ mean the switch is more sensitive to the smoothness of the solution.

Figure 4.31 shows the results on a mesh with $\Delta x/R = 0.4$ at $t = 1.0$, with κ varied from 0.0 to 1.0. As κ was increased from zero numerical instabilities began to appear near the core radius of the vortex. As κ increased these instabilities grew larger and larger. It is interesting to note that the oscillations were always bounded and the solution never

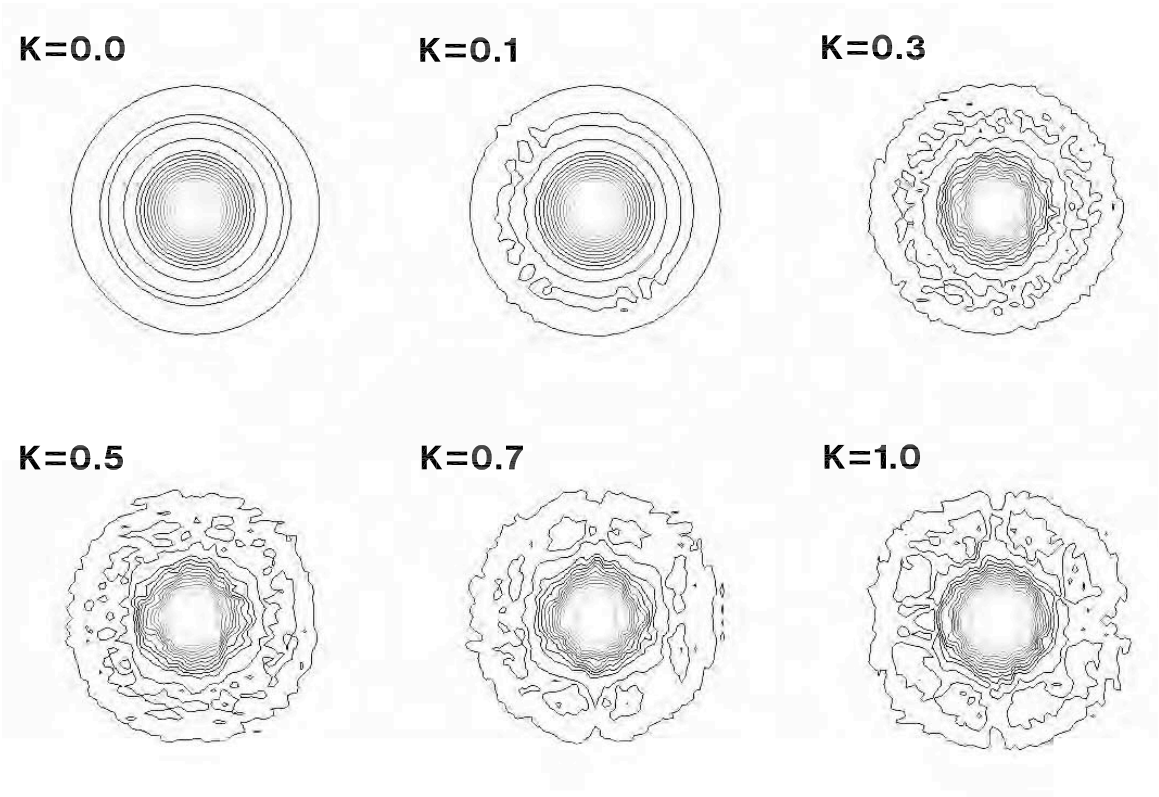

Figure 4.31: Variation in κ parameter for cRoe problem, $\Delta x/R = 0.4$

diverged, but by $\kappa = 0.3$ the solution had degraded quite a bit. The oscillations are most likely due to the scheme performing an incorrect upwind interpolation due to an incorrect switching function. As κ increases the switching function becomes more prone to shifting to the left or right, even when the solution was smooth enough to remain in a central mode. The only value of κ that produced acceptable results was that of $\kappa = 0$, which essentially turns off the upwind interpolation. This result is somewhat expected because the solution is smooth and should never need to use an interpolant other than a central stencil. However, it also shows that the switching function that determines κ is not well formed, and needs to be refined to better measure the smoothness of the stencil. If this switching function were correct, the scheme would always use a central interpolant on the vortex problem regardless of the value of κ chosen.

V. Conclusions

A first-order first upwind method and fourth-order compact difference method were applied to the linear wave equation. The results not only demonstrated that the compact difference is a valid discretization method, but showed that the accuracy and resolving ability of the compact difference is much greater than a first-order method.

The formulation of the compact difference was then modified to use Roe averaged fluxes on the right-hand side and was applied to the one-dimensional shock tube problem. The results confirmed that the order of accuracy of the results matched the order of the left and right variable states used in the flux calculation.

The Compact Adaptive Interpolation scheme of Deng, et. al. [3], or cRoe scheme, was then incorporated into the one-dimensional solver and applied to the one-dimensional shock tube. Previous results were duplicated, and it was shown that the cRoe method could produce sharper shock captures and closer results to the exact solution than the first-order fRoe and third-order oRoe schemes. The shock tube mesh was refined and it was shown that the cRoe scheme behaved consistently, approaching the exact solution as Δx decreased. It was also shown that the value of the cRoe switch weighting parameter κ needed to be tuned to produce the best solution. $\kappa = 0.3$ appeared to produce the best shock captures with the least oscillations or overshoots.

The cRoe scheme was then extended to two-dimensions and included in a generalized coordinate solver. The scheme was then applied to a two-dimensional shock tube with results similar to the one-dimensional case. Again, it was shown that the method was consistent and approached the exact solution as the mesh was refined. Additionally, the κ switch parameter was varied and shown to have an influence on the quality of the solution.

The cRoe scheme was then applied to a smooth problem involving the advection of a vortical structure on rectilinear and curvilinear meshes. Results were compared to those of the third-order oRoe scheme and the fourth-order cC scheme. The formal order of accuracy of the cRoe scheme was shown to lie somewhere between the third and fourth order, with an order of 3.4 on the rectilinear mesh and 3.8 on the curvilinear mesh. Variation of the κ parameter showed that any value of κ greater than zero produces undesirable results for a smooth problem.

5.1 Strengths of the cRoe scheme

The first important conclusion with regards to the cRoe scheme is that it is a consistent scheme in one and two dimensions, and therefore is a valid approximation to the Euler equations. If the scheme were not consistent it would not be able to model the physical behavior described by the governing equations. Although the formal order of accuracy of the cRoe scheme appears to be slightly less than that of the cC compact scheme, the absolute error is comparable. Both the order of accuracy and absolute error of the cRoe scheme were better than that of the third-order oRoe scheme.

The real strength of the cRoe scheme is that it has an absolute error comparable to a standard compact difference method, but it can be applied to solutions with discontinuities. The performance of the cC compact scheme was not measured on the one or two dimensional shock tube problems because the method is unconditionally unstable near discontinuities. The cRoe scheme was able to produce better results than the oRoe scheme, and do so without the use of limiters or filters.

5.2 Weaknesses of the cRoe scheme

The quality of the results from the cRoe scheme depended greatly on the value of the κ switching parameter. There was a slight dependence on the value of κ when the solution had a discontinuity, but a large dependence when the solution was smooth. The fact that the interpolation needed to be set to a pure central difference when the solution was smooth was expected, but the switching method of the scheme should have been able to do this on it's own without setting $\kappa = 0$.

While the cRoe method did improve the accuracy of the solution over the oRoe case, it also added a considerable number of computations per time step. For each conserved variable, the cRoe scheme must solve two implicit systems across the entire domain: one for the left and right variable states, and another for the flux derivative calculations each time step. These implicit systems are large systems of linear equations which can be computationally expensive to solve. The cRoe scheme always took the longest time to solve the advecting vortex problem. The cC scheme was second and the oRoe method the fastest.

For a large domain with many grid points the difference in number of computations could increase the solution time dramatically.

5.3 Relative Computational Costs

The cC and cRoe schemes had a higher computational cost than the oRoe scheme due to the implicit calculations involved. The cC scheme had to solve the implicit flux calculation each Runge-Kutta stage, while the cRoe method solved both the implicit variable state problem and the implicit flux problem each Runge-Kutta stage. However, the order of accuracy determinations proved that the cC and cRoe methods had a lower absolute error than the oRoe method. This means the cC and cRoe methods could be applied to a coarse grid and produce errors comparable to the oRoe method applied to a fine grid. Numerically it was shown that the oRoe method on the $\Delta x/R$=0.2 mesh produced similar results as the cC and cRoe methods on the $\Delta x/R$=0.4 mesh. For a complex problem, it is conceivable the additional expense of the cC and cRoe methods could be offset due to the reduced number of mesh points. This was not the case with the advecting vortex results, as the solution times for the cC and cRoe methods took 11% and 18% longer than the oRoe cases, respectively.

5.4 Future Work

The next step to validating this new cRoe scheme would be to apply it to the full Navier-Stokes equations and use it to solve a viscous problem such as a flat plate boundary layer. The numerical results could then be compared to the Blasius solution for accuracy. The addition of viscosity would add another level of difficulty to the solution. Since viscous effects occur on a scale much smaller than convective effects the resolution ability of the compact schemes could be investigated. In order to maintain a global order of accuracy the viscous fluxes of the Navier-Stokes equations should be calculated to the same or greater order of accuracy as the convective fluxes. For the cC and cRoe schemes this could be accomplished using similar compact difference formulations.

Another important problem that should be considered would be one involving a standing discontinuity, such as a high Mach number blunt-body or a ramp with an oblique shock.

The shock tube problem demonstrated the ability of the cRoe method to handle a discontinuous solution on a transient problem. It is often more difficult for numerical solutions to resolve a stationary discontinuity than a moving one without excessive smearing or broadening. For error comparison purposes there exists experimental data on blunt bodies and an exact analytical solution for oblique shock problems.

Finally, any refinements that could be made to the adaptive interpolation method would be an improvement. For the method to be more robust the interpolation should be able to better gauge the smoothness of the function without a manual adjustment of the value of κ. Several flux splitting schemes, such as Edward's Low Diffusion Flux Splitting Scheme [4], have logic incorporated into them to determine sonic transitions and contact surfaces for proper upwinding. If similar logic could be included in the cRoe method, the robustness of the scheme would be greatly increased.

5.5 Final Conclusion

The cRoe scheme proposed by Deng and Maekawa [3] is a consistent compact difference scheme with near fourth-order accuracy. It was shown to capture discontinuities and gradients in a shock tube problem better than a third-order Roe scheme, and was also able to produce absolute errors similar to that of a standard compact scheme on a smooth problem. While its robustness could be improved through a better interpolant switching parameter, it successfully produced a nonoscillatory result on a discontinuous solution using an unfiltered compact difference method.

Bibliography

1. Anderson, J. D. *A History of Aerodynamics*. Cambridge, 1997.
2. Blazek, J. *Computational Fluid Dynamics: Principles and Applications*. Elsevier, 2004.
3. Deng, Xiaogang and Hiroshi Maekawa. "Compact High-Order Accurate Nonlinear Schemes," *Journal of Computational Physics*, *130*:77–91 (1997).
4. Edwards, J.R. "A Low Diffusion Flux Splitting Scheme for Navier Stokes Calculations," *Computers and Fluids*, *26*:653–659 (1997).
5. Gaintonde, D.V. and M. R. Visbal. "Further Development of a Navier-Stokes Solution Procedure Based on Higher-Order Formulas." *Proceedings of the 37th AIAA Aerospace Sciences Meeting and Exhibit*. Reno, NV: AIAA, 1999.
6. Gaitonde, D. Unpublished correspondence with D. Gaitonde, 2005.
7. Gottlieb, D. Unpublished correspondence.
8. Harten, A. and J.M.Hyman. "Self Adjusting Grid Methods for One-Dimensional Hyperbolic Conservation Laws," *Journal of Computational Physics*, *18*(2):235–269 (1983).
9. Hartin, A., et al. "Uniform High-Order Accurate Essentially Non-Oscillatory Schemes, III," *Journal of Computational Physics*, *71*:213 (1987).
10. Hirsch, C. *Numerical Computation of Internal and External Flows, Volume 1*. John Wiley and Sons, 1990.
11. Hirsch, C. *Numerical Computation of Internal and External Flows, Volume 2*. John Wiley and Sons, 1990.
12. Hoffman, Klaus A. and Steve T. Chaing. *Computational Fluid Dynamics Volume III* (4th Edition). Wichita, Kanas, 67208-1078 USA: Engineering Education System, 2000.
13. Jameson, A., et al. "Numerical Solutions of the Euler Equations by Finite Volume Methods Using Runge-Kutta Time-Stepping Schemes," *AIAA Paper*, (81-1259) (1981).
14. Lax, P. and B. Wendroff. "Systems of Conservation Laws," *Commun. Pure Appl. Math*, *13*:217–237 (1960).
15. Lele, S.K. "Compact Finite Difference Schemes with Spectral Like Resolution," *Journal of Computational Physics*, *103*:16–42 (1992).
16. Orszag, S. and M. Israeli. "Numerical Simulation of Viscous Incompressible Flows," *Annual Review of Fluid Mechanics*, *6*:281–318 (1974).
17. Poinsot, T.J. and S.K. Lele. "Boundary Conditions for Direct Simulation of Compressible Viscous Flows," *Journal of Computational Physics*, *101*(1):104–129 (1992).
18. Ravichandran, K.S. "Higher Order KFVS Algorithms Using Compact Upwind Difference Operators," *Journal of Computational Physics*, *130*:161–173 (1997).
19. Roe, P.L. "Approximate Riemann Solvers, Parameter Vectors, and Difference Schemes," *Journal of Computational Physics*, *43*:357–372 (1981).

20. Sod, G. A. "A Survey of Several Finite Difference Methods for Systems on Non-linear Hyperbolic Conservation Laws," *Journal of Computational Physics*, *27*:1–31 (1978).

21. Tannehill, J. C., et al. *Computational Fluid Mechanics and Heat Transfer* (Second Edition). Philadelphia: Taylor and Francis, 1997.

22. VanLeer, B. "Towards the Ultimate Conservative Difference Scheme V. A Second Order Sequel to Godunov's Method," *Journal of Computational Physics*, *32*:101–136 (1979).

23. Vatsa, V.N. and J.L.Thomas. "Navier-Stokes Computations of Prolate Spheroids at Angle of Attack." *Proceedings of the AIAA Atmospheric Flight Mechanics Conference*. Monterey, CA: AIAA, 1987.

24. Visbal, M. R. and D.V. Gaintonde. "High-Order-Accurate Methods for Complex Unsteady Subsonic Flows," *AIAA Journal*, *37*(10):1231–1239 (1999).

25. White, F. *Viscous Fluid Flow*. Boston: McGraw Hill, 1991.

Vita

First Lieutenant Barry A. Croker was born in Dover, New Hampshire and graduated from Oyster River High School in 1996. He entered undergraduate studies at Utah State University in Logan, UT, where he graduated with a Bachelor of Science in Mechanical Engineering and was commissioned in May of 2000.

His first Air Force assignment was to the Gas and Chemical Laser Branch, Laser Division, Directed Energy Directorate, Air Force Research Laboratory, as an Advanced Chemical Oxygen-Iodine Laser Test Engineer. There he served as the Program Manager and Test Engineer for the Advanced Tactical Laser 1-mol Demonstrator.

In August of 2003, he entered the Aeronautical Engineering program at the Graduate School of Engineering and Management, Air Force Institute of Technology. His academic focus areas were Computational Fluid Dynamics and Aerodynamics. Upon graduation, he will be assigned to the Computational Research Branch, Aeronautical Sciences Division, Air Vehicles Directorate, Air Force Research Lab at Wright-Patterson AFB, OH where he will continue his work in the field of computational fluid dynamics.

First Lieutenant Croker is married and has three children.

REPORT DOCUMENTATION PAGE

Form Approved
OMB No. 0704–0188

1. REPORT DATE *(DD–MM–YYYY)*	2. REPORT TYPE	3. DATES COVERED *(From — To)*
21–03–2005	Master's Thesis	Sep 2003 — Mar 2005

4. TITLE AND SUBTITLE

Development of a Higher-Order Upwind Algorithm for Compressible Fluid Flow

5a. CONTRACT NUMBER

5b. GRANT NUMBER

5c. PROGRAM ELEMENT NUMBER

6. AUTHOR(S)

Croker, Barry A., 1LT, USAF

5d. PROJECT NUMBER

2003-014

5e. TASK NUMBER

5f. WORK UNIT NUMBER

7. PERFORMING ORGANIZATION NAME(S) AND ADDRESS(ES)

Air Force Institute of Technology
Graduate School of Engineering and Management (AFIT/ENY)
2950 Hobson Way
WPAFB OH 45433-7765

8. PERFORMING ORGANIZATION REPORT NUMBER

AFIT/GAE/ENY/05-M05

9. SPONSORING / MONITORING AGENCY NAME(S) AND ADDRESS(ES)

AFOSR/NA
Dr. John Schmisseur
801 N. Randolph Street, Rm 732
Arlington VA 22203-7765

10. SPONSOR/MONITOR'S ACRONYM(S)

11. SPONSOR/MONITOR'S REPORT NUMBER(S)

12. DISTRIBUTION / AVAILABILITY STATEMENT

Approval for public release; distribution is unlimited.

13. SUPPLEMENTARY NOTES

14. ABSTRACT

A global fourth-order solution method that incorporates compact differencing with Roe's approximate Riemann solver was investigated. This method was incorporated into a one-dimensional numerical simulation of the compressible Euler equations, and applied to a one-dimensional shock tube problem. The method was also extended to two dimensions, and applied to a two-dimensional shock tube problem and an advecting vortical structure problem on both rectilinear and curvilinear meshes. The results were compared to a third-order Roe scheme and a fourth-order compact difference scheme. An order of accuracy determination showed that it has an order of accuracy somewhere near fourth order, with absolute error comparable to that of the standard compact difference scheme. With proper selection of solution parameters, the scheme was also shown to accurately capture a discontinuous solution where unfiltered compact schemes would become unstable.

15. SUBJECT TERMS

Difference Equations, Euler Equations, Computational Fluid Dynamics, Numerical Methods and Procedures

16. SECURITY CLASSIFICATION OF:			17. LIMITATION OF ABSTRACT	18. NUMBER OF PAGES	19a. NAME OF RESPONSIBLE PERSON
a. REPORT	b. ABSTRACT	c. THIS PAGE			Richard J. McMullan, Maj, USAF (ENY)
U	U	U	UU	98	19b. TELEPHONE NUMBER *(include area code)* (937) 255–3636, ext 4559